DOT/FAA/AR-04/16

Office of Aviation Research
Washington, D.C. 20591

Uncontained Engine Debris Analysis Using the Uncontained Engine Debris Damage Assessment Model

September 2004

Final Report

U.S. Department of Transportation
Federal Aviation Administration

NOTICE

Technical Report Documentation Page

1. Report No.	2. Government Accession No.	3. Recipient's Catalog No.
DOT/FAA/AR-04/16		

4. Title and Subtitle	5. Report Date
UNCONTAINED ENGINE DEBRIS ANALYSIS USING THE UNCONTAINED ENGINE DEBRIS DAMAGE ASSESSMENT MODEL	September 2004
	6. Performing Organization Code 418300D
7. Author(s) Silvia Seng, John Manion, and Chuck Frankenberger	8. Performing Organization Report No.
9. Performing Organization Name and Address Naval Air Warfare Center, Weapons Division 1 Administration Circle China Lake, CA 93555-6100	10. Work Unit No. (TRAIS) 11. Contract or Grant No. Interagency agreement DTFA03-01-X-900013
12. Sponsoring Agency Name and Address U.S. Department of Transportation Federal Aviation Administration Office of Aviation Research Washington, DC 20591	13. Type of Report and Period Covered Final Report 14. Sponsoring Agency Code ANM-100

15. Supplementary Notes

The FAA William J. Hughes Technical Center Monitor was Donald Altobelli.

16. Abstract

As part of the Federal Aviation Administration's (FAA) Aircraft Catastrophic Failure Prevention Program, the Naval Air Warfare Center was tasked to examine and evaluate the Uncontained Engine Debris Damage Assessment Model (UEDDAM). UEDDAM was written to provide a standardized tool for uncontained engine rotor failure analysis. This study was conducted to exercise the code and evaluate its usefulness in performing rotor burst analysis on a small generic business jet and a generic twin-engine aircraft. This evaluation also supported the Aviation Rulemaking Advisory Committee, Power Plant Installation Harmonization Working Group activities.

This report explains the analysis methodology, results, and trade studies performed using UEDDAM. Though the aircraft used in the study do not represent a specific aircraft, industry input was used to create the input data required so that the results would be comparable to a real aircraft analysis.

17. Key Words	18. Distribution Statement
Engine, Debris, Damage model, Engine fragment, Generic aircraft, UEDDAM	This document is available to the public through the National Technical Information Service (NTIS), Springfield, Virginia 22161.

19. Security Classif. (of this report)	20. Security Classif. (of this page)	21. No. of Pages	22. Price
Unclassified	Unclassified	75	

TABLE OF CONTENTS

LIST OF FIGURES

LIST OF TABLES

LIST OF ACRONYMS

AC	Advisory Circular
ARAC	Aviation Rulemaking Advisory Committee
CAD	Computer-aided design
CFR	Code of Federal Regulations
COVART	Calculation of Vulnerable Area
DFM	Debris Fragment Model
DISK1	Single disk
DSKFR	Single small fragment and a single 1/3 disk section
FAA	Federal Aviation Administration
FASTGEN	Fast Target Generation Model
GBJ	Generic business jet
GT	Generic twin-engine aircraft
HPC	High-pressure compressor
HPT	High-pressure turbine
LPC	Low-pressure compressor
LPT	Low-pressure turbine
MFRAG	Intermediate size fragment
MULTI	Multiple fragments
NAWC-WD	Naval Air Warfare Center, Weapons Division
P_{haz}	Average probability of hazard of component
P_{HAZ}	Probability of catastrophic hazard to the aircraft
$P_{haz/h}$	Probability of catastrophic hazard, given a hit
PPIHWG	Power Plant Installation Harmonization Working Group
SINGL	Single small fragment
UEDDAM	Uncontained Engine Debris Damage Assessment Model

EXECUTIVE SUMMARY

As part of the Federal Aviation Administration Aircraft Catastrophic Failure Prevention Program, the Naval Air Warfare Center was tasked to examine and evaluate the Uncontained Engine Debris Damage Assessment Model (UEDDAM). UEDDAM was written to provide a standardized tool for uncontained engine rotor failure analysis. This study was conducted to exercise the code and evaluate its usefulness in performing rotor burst analysis on a small generic business jet and a generic twin-engine aircraft. This evaluation also supported the Aviation Rulemaking Advisory Committee, Power Plant Installation Harmonization Working Group activities.

This report explains the analysis methodology, results, and trade studies performed using UEDDAM. Though the aircraft used in the study do not represent a specific aircraft, industry input was used to create the input data required so that the results would be comparable to a real aircraft analysis.

1. INTRODUCTION.

1.1 PURPOSE.

Although the condition of aircraft engine rotors are regularly monitored, uncontained disk burst events still occur worldwide. Uncontained rotor failures can be caused by various reasons including fatigue and internal and external foreign object debris.

Under the Federal Aviation Administration (FAA) Aircraft Catastrophic Failure Prevention Program, the Naval Air Warfare Center, Weapons Division (Systems Vulnerability Branch/Code 418300D) at China Lake, CA, (NAWC-WD) has developed an analysis tool to evaluate the probability of hazard to an aircraft given engine rotor failure. To address this tasking, NAWC-WD has teamed with SURVICE Engineering to develop a computer program called the Uncontained Engine Debris Damage Assessment Model (UEDDAM). The model is intended to aid the design and certification of aircraft, providing a standardized tool (methodology) to conduct rotor burst assessments. As part of that effort, a generic business jet (GBJ) and a generic twin-engine aircraft (GT) were evaluated for engine rotor burst using UEDDAM. These studies were intended to refine the analysis process and examine the capabilities of UEDDAM.

This report describes the methodology, analysis, and trade studies performed using UEDDAM, as well as lessons learned and an evaluation of UEDDAM capabilities.

1.2 BACKGROUND.

The UEDDAM code was developed to address an industry-FAA need for an analytical tool capable of conducting rotor burst assessment that incorporates fragment penetration, system level hazard assessment, and multiple debris fragments. UEDDAM was developed as a design tool capable of conducting aircraft configuration trade studies and as certification tool to show compliance with Title 14 Code of Federal Regulations (CFR) 25.903(d)(1). UEDDAM is based on vulnerability assessment codes used in industry during aircraft design and development to minimize the vulnerability of military aircraft to ballistic threats.

UEDDAM is a wrap around code for the vulnerability assessment codes Fast Target Generation Model (FASTGEN) and a modified version of the Calculation of Vulnerable Area and Repair Time (COVART). Modifications to COVART include modified penetration equations more suited to disk and blade fragments than the existing penetration equation. All further references to COVART will refer to this modified version. UEDDAM allows the analyst to accurately model an uncontained engine failure through use of the aircraft geometry, debris characteristics, and conducting a Monte Carlo analysis. Given the debris definition and aircraft geometry, UEDDAM uses FASTGEN to develop debris fragment trajectories through the aircraft. COVART provides penetration assessment based on the debris characterizations and summarizes the component contribution to aircraft hazard level for a given release origin. The results from COVART are accumulated by UEDDAM for multiple iterations of fragment trajectories from a release origin, multiple release origins about the circumference of the rotor disk, and multiple rotor assemblies. UEDDAM generates hazard probability output for each event in summary format and also provides details of critical component contributions for each Monte Carlo

iteration, or as a tabulation of risk angles for each critical component per event. Debris types may be assessed independently or together as a single evaluation of the hazard for specified debris uncontained event.

As a design tool, UEDDAM can provide early insight to the rotor burst hazard for a given aircraft configuration. Early in the aircraft development cycle a simple aircraft geometry can be developed using the FASTGEN primitive modeling elements. Aircraft skin, major structural elements, and flight critical components are easily modeled to provide a reasonable representation of the aircraft configuration. During this phase of an aircraft development program, the design is very fluid. A simple approach should be taken to model the configuration so that design trade studies can be conducted quickly. The use of very detailed models during the early development phase will significantly hamper the analyst's ability to respond to configuration changes. Keeping the aircraft model simple, the analyst can conduct design trade studies to address rotor burst hazard minimization. Additional detail should be added to components showing high hazard contribution to refine the analysis. As the aircraft design matures, the model fidelity can be increased as detailed component information becomes available and as further analysis warrants.

As a certification tool, UEDDAM provides a standardized approach to conduct rotor burst hazard assessment. UEDDAM output provides insight to the rotor burst hazard in several ways. UEDDAM output can be used to develop a top level 1 in 20 analysis to address compliance to CFRs. It also provides specific details at the system and component level. The output can be categorized by rotor or debris category, providing a high level of flexibility in viewing analysis results. Through the use of UEDDAM as a design tool, a history of trade study results can be used to support the minimization intent of the rule.

It is well understood that a rotor burst analysis is a complex analysis. UEDDAM was developed to provide useful tools to aide in conducting the analysis and presenting the results. A UEDDAM Visualizer was developed, which provides visualization of the complex data and information generated from a UEDDAM run. It allows visualization of the aircraft geometry, debris hazard zones, debris trajectories, probability plots of the hazard levels, and translational risk angles.

1.3 RELATED DOCUMENTS.

The following documents relate to this report:

a. FAA Advisory Circular 20-128A, "Design Considerations for Minimizing Hazards Caused by Uncontained Turbine Engine and Auxiliary Power Unit Rotor and Fan Blade Failures."

b. "Uncontained Engine Debris Damage Assessment Model (UEDDAM) Version 2.0 User's Manual," SURVICE Engineering, SURVICE TR-02-020 October 2002.

c. "Uncontained Engine Debris Damage Assessment Model (UEDDAM) Visualizer Beta Version User's Manual," SURVICE Engineering, SURVICE 00-017, December 2000.

d. DOT/FAA/AR-99/119, "Large Engine Uncontained Debris Analysis," Naval Air Warfare Center, Weapons Division, October 1998.

2. DISCUSSION.

2.1 OBJECTIVE.

The objective for this study was to demonstrate the capabilities of the UEDDAM code. Through this process, an analysis was conducted that illustrates how UEDDAM can be used to address current Advisory Circular (AC)20-128A methodologies, in addition to providing a design tool to conduct trade studies aimed at mitigating the uncontained engine debris hazard. Two generic aircraft models were defined: a generic twin-engine aircraft and a generic business jet. To ensure that the generic aircraft were representative, industry input was used in the construction of the FASTGEN geometric target models, fault trees, and multiply vulnerable component list.

2.2 DEFINITIONS AND NOMENCLATURE.

Several terms are used in this report to describe the analysis that are not self-explanatory. This section will discuss what is meant by these terms.

A rotor burst analysis is conducted using several debris scenarios: a single disk segment, single blade fragment, or multiple fragments. The debris category is a name used to define the type of analysis being conducted (i.e., for a single disk analysis the debris category used is DISK1, for multiple fragments, the debris category is MULTI.) The debris types are a description used by UEDDAM to distinguish how the fragment will be defined. There are three debris types: small fragments, large fragments, and sections. So, a single small fragment debris category (SINGL) may consist of a single small fragment, and a multiple fragment debris category (MULTI) may consist of a 1/3 disk section and 12 small fragments.

The small fragment debris type refers to fragments that are small enough to be sufficiently defined by a single shotline. The size of these fragments are described by height, width, and thickness. The large fragments are also described by height, width, and thickness, but are too large for a single shotline to represent the path of the debris. Therefore, a grid is constructed within the fragment presented area. The grid spacing is defined by the user in the debris record. The center of the grid is the centroid of the presented area. The grid lines are parallel lines mapped relative to the fragment centroid. A shotline will originate at each point on the resulting grid. The shape of the section debris type is defined by the arc of the segment (in degrees) and the inner and outer radii. The grid spacing is defined in the debris record and are mapped as parallel gridlines and drawn outward from the centroid (figure 2-1).

UEDDAM was run for each combination of flight phase, aircraft engine, rotor stage, and uncontained debris category. Each of the individual runs will be referred to as a case. A run will refer to a single execution of UEDDAM whereas a production run will indicate all the runs required to produce the output for all combinations of flight phase, rotor, engine, and debris category for a given aircraft configuration.

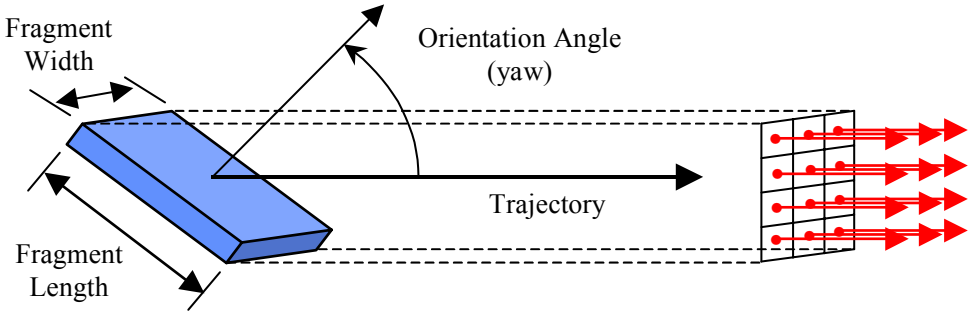

FIGURE 2-1. SHOTLINE GRID DEFINITION

The probability of catastrophic hazard to the aircraft will be denoted as P_{HAZ}. P_{HAZ} is the 1-in-20 value specified in AC 20-128A and is specific to a particular debris category. The rotor, flight phase, or engine average probability of hazard will be identified by describing the level of averaging and P_{haz} (lowercase subscript), for example, Engine 1 average P_{haz}.

3. ANALYSIS APPROACH.

3.1 ANALYSIS OBJECTIVES.

The objectives for the analysis for the two generic aircraft were to determine the probability of catastrophic hazard given an uncontained engine event (P_{HAZ}) for each aircraft, determine the major contributors to the P_{HAZ}, and perform trade studies to minimize the contributions of those components to the P_{HAZ}.

3.2 TARGET DESCRIPTIONS.

The aircraft geometric representations are called the geometric target models and were created using FASTGEN4. Some of the components were excluded from the geometric target models because the component was noncritical and did not significantly reduce the fragment velocity, such as the interior wall panels.

3.2.1 Generic Business Jet.

The geometric target for the GBJ comprises 11.5 ft behind the aft pressure bulkhead (figure 3-1) of the aircraft. The engines are small, high-bypass ratio turbofan engines mounted on the aft fuselage. Each engine consists of nine rotors: the fan and low-pressure compressor (LPC1 and LPC2); three-stage, high-pressure compressor (HPC1, HPC2, and HPC3); one stage, high-pressure turbine (HPT1); and a three-stage, low-pressure turbine (TLP1, TLP2, and TLP3—the nomenclature was changed because LPT is a computer-reserved word). Some of the components included in the target model are the fuselage frames, longerons, skin, engine beams, fuel supply lines, fuel motive lines, control cables, nacelles, engine case, and the aft pressure bulkhead. The forward fuselage was not included because the forward-most spread angle did not intersect any components forward of the aft pressure bulkhead.

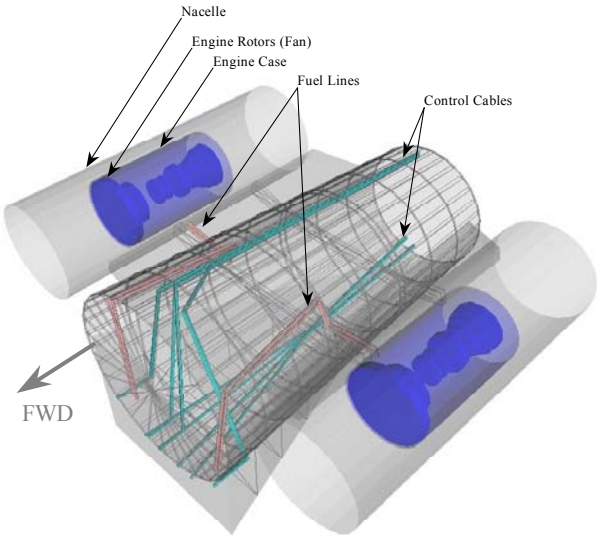

FIGURE 3-1. GENERIC BUSINESS JET TARGET GEOMETRY

3.2.2 Generic Twin-Engine Aircraft.

The GT geometric target consisted of the fuselage of a wing-mounted twin-engine aircraft (figure 3-2). The engines are large, high-bypass ratio turbofans. Each engine consisted of 18 rotors. The systems included in the geometric target model are the fuel, hydraulic, and flight control systems, including pumps, actuators, mixers, cables, and supply and return lines. Fuselage and wing fuel tanks were included as well as the fuel motive lines. The aircraft structure included frames and longerons in the fuselage and a more complex wing structure. Because damage to a spar web did not result in failure of the spar unless several other components were damaged as well, the spars were split into the upper spar cap, web, and lower spar cap. Although seating and main cabin furniture and fixtures were not included, the cabin floor was included.

The fuselage skin was created in a three-dimensional computer-aided design (CAD) program. Small triangles were used to provide the contours of the skin when converting the skin from the CAD program to FASTGEN4 geometry. The number of elements (triangles) generated by the conversion often result in large file sizes of as much as two orders of magnitude greater than those constructed using the simple geometric shapes available in FASTGEN such as cylinders, cones, and rectangular boxes. Therefore, many of the components for the GT were created using the FASTGEN4 primitives.

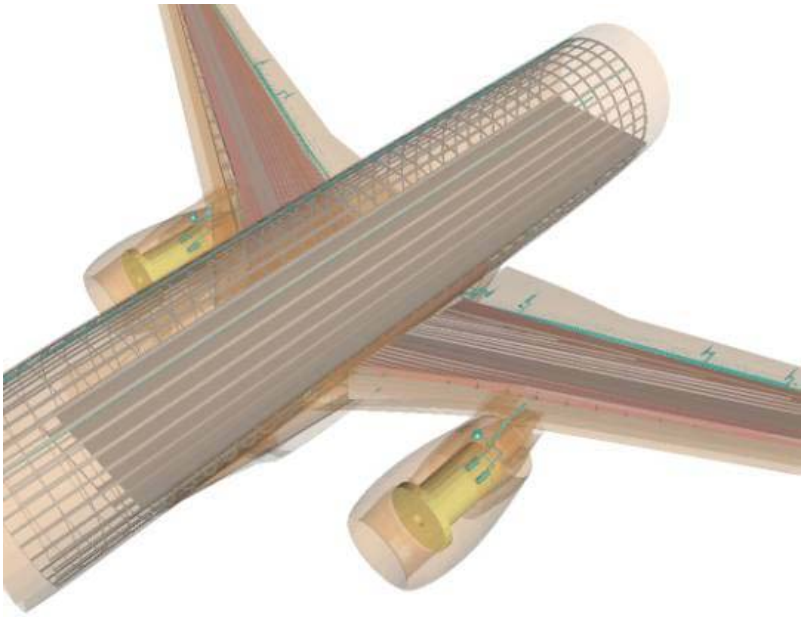

FIGURE 3-2. GENERIC TWIN TARGET GEOMETRY

3.3 ANALYSIS PARAMETERS.

The following input parameters and assumptions were used for both the GBJ and GT aircraft UEDDAM analyses.

3.3.1 Flight Phase Probability of Failure.

Rotor burst analyses were conducted for catastrophic hazards to the aircraft. Because component criticalities can vary with flight phase, the criticality of each component was defined for each flight phase. The breakdown of flight phases was based on the accepted industry standards for a commercial aircraft flight profile but reduced to six phases (a COVART limitation). The modified phase grouping was based on common component phase criticalities and is slightly different for the GBJ and GT. Table 3-1 describes the phases of flight and flight phase probability of failure.

TABLE 3-1. FLIGHT PHASES AND FLIGHT PHASE FAILURE DISTRIBUTION

Generic Business Jet		Generic Twin-Engine Jet	
Phase of Flight	Flight Phase Failure Distribution	Phase of Flight	Flight Phase Failure Distribution
Takeoff to before V1	35%	Takeoff to before V1	35%
V1 to First Power Reduction	20%	V1 to First Power Reduction	20%
Initial Climb	22%	Climb	22%
Final Climb, Cruise, and Initial Descent	14%	Cruise	14%
Approach and Landing	7%	Descent	3%
Landing Roll	2%	Approach, Landing, and Reverse	6%

3.3.2 Debris Characteristics.

The Debris Fragment Model (DFM) for high-bypass ratio turbofan engines (table 3-2) was developed by NAWC-WD during previous Aviation Rulemaking Advisory Committee (ARAC) activities and was used to determine debris characteristics for both the GBJ and GT engines in this report. The DFM is based on historical data from in-service rotor burst events. In most cases the DFM trajectory spread angles exceeded the minimum requirements of the AC 20-128A. A comparison of the DFM and AC 20-128A fragment characteristics was conducted using the GBJ model geometry. The results are discussed in section 4.2.2.1. The latest version of the debris fragment model is included in appendix A.

TABLE 3-2. HIGH-BYPASS RATIO ENGINE FRAGMENT CHARACTERIZATION

Component	Number of Fragments (Average/Event)	Normalized Size	Weight lbs (% of total)	Velocity (ft/sec) at 0° plane	Spread Angle Degrees
Fan					
Blade Event (Helical)	5.25	25%	1.8 (20%)	713	+21 to -35
Disk Event					
Blades	27.7	25%	1.8 (20%)	813	+15 to -30
Disks	3	100%	45 (38%)	303	+2 to -3
Compressor					
Blade Event					
Spacer – Rim					
Blades	6.5	100%	0.25 (100%)	642	+15 to -3
Rim	2	80%	6.0 (30%)	523	+15 to 0
Disk Event					
Blades	4.5	50%	0.19 (76%)	609	+5 to -25
Disk (Large Fragment)	1	85%	9 (45%)	380	+5 to -5
Disk (Intermediate Fragment)	1	30%	4 (20%)	385	+10 to -5
HP Turbine					
Blade Event	10	80%	0.25 (100%)	337	+20 to -50
Spacer-Rim					
Blades	11	85%	0.25 (100%	871	+15 to -40
Rim	1	50%	10 (83%)	967	0 to -12
Spacer	1	50%	2 (16%)	781	+20 to -37
Disk Event					
Blades	12	70%	0.25 (100%)	871	+15 to -60
Disk	1	30%	10 (8%)	967	+3 to -11
LP Turbine					
Blade Event	6.5	50%	0.25 (37%)	212	+20 to -45
Blade Event Last Stage	6.5	50%	0.25 (37%)	200	0 to -75
Spacer-Rim					
Blades	5	15%	0.05 (7%)	326	+6 to -20
Rim	1	20%	11.3 (9%)	505	+5 to -5
Disk Event					
Blades	5	28%	0.25 (20%)	313	+5 to -40
Disk	1	20%	18 (15%)	535	+3 to -5

+ angles are forward, - angles are aft of the rotor plane of rotation
Note: See appendix A for the latest fragment model, this table has been superseded

The DFM describes the debris fragments in nondimensional terms for each engine section, such as fan blade size as a percentage of the full blade length. These nondimensional values were applied to each rotor to determine the size and mass of the fragments used in this analysis.

The following debris categories were used in the analysis of the GBJ and GT.

- DISK1—a single 1/3 disk section of the rotor representing a disk event
- MFRAG—an intermediate sized fragment representing a rim event
- MULTI—a single 1/3 disk section and multiple small fragments representing a disk event
- SINGL—a single small fragment, representing a blade event
- DSKFR—a single small fragment and a single 1/3 disk section
- MULTI3—three 1/3 disk fragments and associated small fragments for 1 of the 1/3 sections

At the recommendation of the 28th ARAC, Power Plant Installation Harmonization Working Group (PPIHWG) meeting participants, the last two debris categories were not used for the trade studies. This reduction in debris categories was made to reduce the number of analysis cases.

The debris characterization for the AC 20-128A suggested debris categories uses the same spread angles for all engine sections. (Figures 3-3 and 3-4 show the spread and release angle definitions.) AC 20-128A recommends that spread angles of ±3º be used for 1/3 disk cases, ±5º for intermediate sized fragments (rim events) and ±15º for small fragments (blade events). The DFM spread angles are defined by engine section for each debris category. Table 3-3 shows a comparison of the DFM-recommended debris characterization and the AC 20-128A recommended values. In most cases, the DFM spread angles are larger than the FAA recommendations; however, the three boxes highlighted in table 3-3 (1/3 disk and intermediate fragment events for the fan and the small fragments from the compressors spread angles) indicate spread angles lower than those suggested by the AC 20-128A. Also, in some cases, the DFM suggested angles are shifted forward or aft of the existing AC 20-128A values. However, because of the overlap in the hazard zones of multiple rotors, the overall coverage for the DFM spread angles is greater than that of the AC.

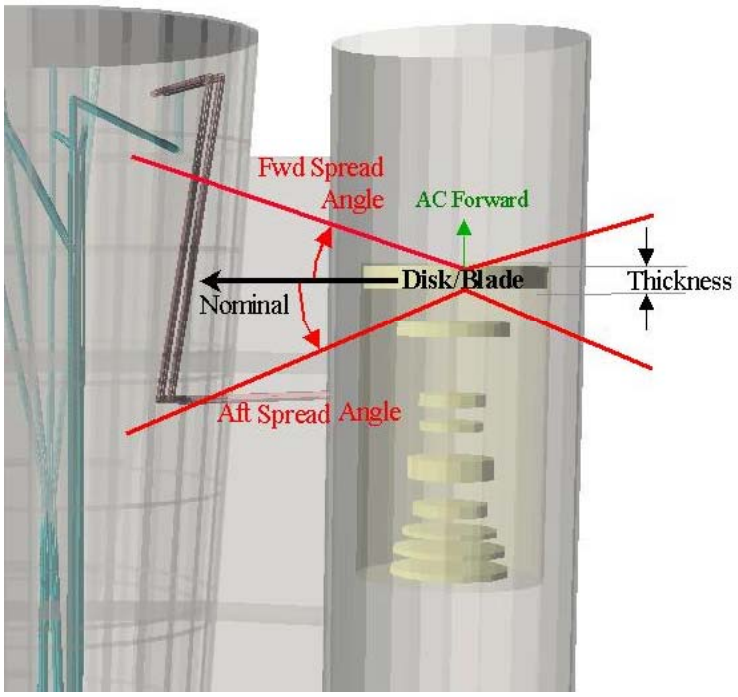

FIGURE 3-3. FORWARD AND AFT SPREAD ANGLE DEFINITION

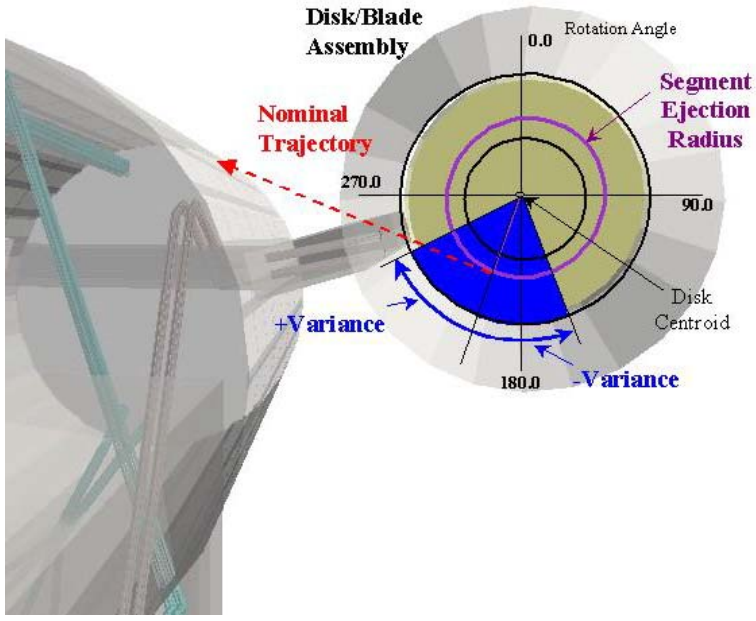

FIGURE 3-4. TRANSLATIONAL ANGLE LIMITS DEFINITION

TABLE 3-3. COMPARISON OF DFM AND AC 20-128A SPREAD ANGLES

	Disk Event (1/3 Disk)		Rim Event (Intermediate Fragment)		Blade Event (Small Fragment)	
	DFM	AC20-128	DFM	AC20-128	DFM	AC20-128
FAN	+2º/-3º	+3º/-3º	+2º/-3º	+5º/-5º	+21º/-35º	+15º/-15º
LPC	+5º/-5º		+10º/-0º		+15º/-3º	
HPC						
HPT	+3º/-11º		+0º/-12º		+20º/-50º	
LPT	+3º/-5º		+5º/-30º		+20º/-45º	

3.3.3 Near-Field Components.

UEDDAM uses the near-field file to list event-engine specific components that are close to the engine (within the nacelle). The DFM defines fragment velocities after exiting the nacelle; therefore, the nacelles, engine case, and engine-mounted accessories were placed in the near-field file. Thus, those components defined in the near-field file do not reduce the energy of the debris fragments.

3.3.4 Autofail Components.

UEDDAM uses the autofail file to define an event-engine specific list of components that would be nonfunctional as a result of an uncontained engine event. For example, generators that are run by the engine or other accessories dependent on bleed air may not function following a rotor burst, even if they were not hit by debris. The rotors and critical engine-mounted accessories for each aircraft were listed in the autofail file.

3.3.5 Probability of Catastrophic Hazard, Given a Hit.

A Failure Modes and Effects Analysis was used to identify critical components and aid in a fault tree analysis. The fault tree analysis was then used to aid the definition of multiply vulnerable groups. The fault tree in figure 3-5 reflects a single phase of flight of the GBJ. This type of analysis was repeated for each phase of flight for both aircraft examined in this analysis.

Critical components were listed in the JTYPE file and assigned to PK tables. The PK tables, specified in the PK file, define the probabilities of catastrophic hazard, given a hit ($P_{haz/h}$). The PK tables consist of several curves that define the component $P_{haz/h}$, given velocity for fragments of different sizes. Each critical component is assigned a PK table; however, each PK table can be used to describe multiple components. Using these tables, COVART interpolates the $P_{haz/h}$ of a component for fragments of any size and velocity. The $P_{haz/h}$ combines the probability of component dysfunction, given a hit ($P_{d/h}$), and the probability of catastrophic hazard, given component dysfunction ($P_{haz/d}$).

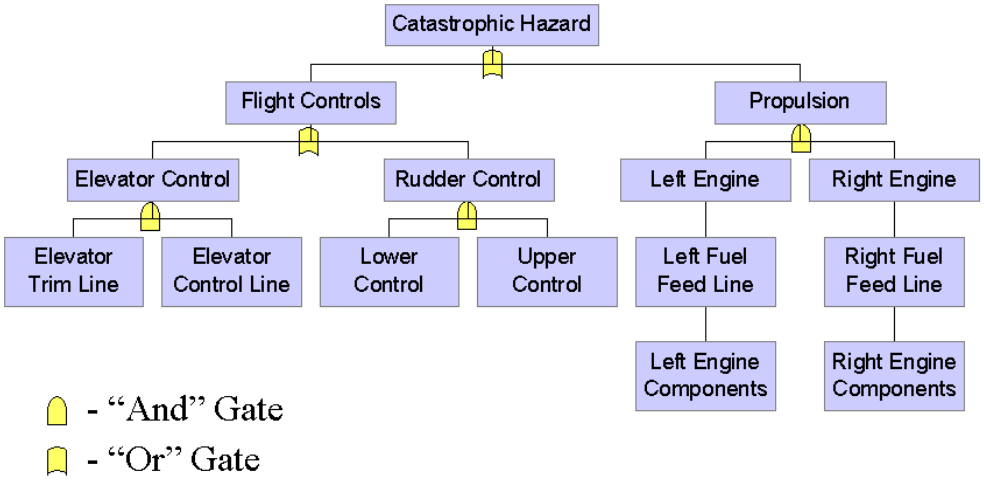

FIGURE 3-5. SAMPLE FAULT TREE (GBJ for V1 to V1 + 30 seconds)

A conservative approach was taken for these analyses, and most critical components hit by fragments with a velocity greater than 2 ft/s were considered dysfunctional ($P_{haz/h} = 1.0$). Larger structural components that were unlikely to be damaged by small fragments were defined in a second PK table that specified that only debris fragments of 7000 grains (1 lb) or larger would result in component dysfunction ($P_{haz/h} = 1.0$).

3.4 OUTPUT.

UEDDAM allows the user to select up to eight output files, as listed below.

1. Hazard Summary—The hazard summary file contains the average P_{haz} of all the iterations for each release angle and hazard level (or flight phase), the average P_{haz} for all the release angles swept by UEDDAM, and the average P_{haz} over 360° of sweep of the release angles. Any angle not swept by UEDDAM is considered to have a P_{haz} of 0. The two averages will be the same if all 360° of possible release angles are swept.

2. Hit Summary—The hit summary file contains the component contributions to P_{HAZ}. The summary contains two averages. The first set of component contributions to P_{haz} values are for the release angles swept by UEDDAM. The second set of values assume that any angles not swept by UEDDAM have a P_{HAZ} of zero and calculate the component contributions for a 360° release angle sweep.

3. Detail File—The detail file is similar to the hit summary file in that it contains the component contributions to P_{HAZ}. However, the component contributions to P_{HAZ} for each iteration are written to this file.

4. Visualizer File—This file is used internally by the UEDDAM Visualizer V1.0 and contains shotline information.

5. Intercept File—This file contains component translational and forward and aft spread risk angles for each component. The file contains comma-separated values and is easiest to understand if opened in Excel. These intercept angles are calculated independently of any of the shotlines.

6. Trajectory File—This file contains fragment release and shotline orientation data. The file also lists the release point (x,y, and z-location), and ray orientation (yaw and roll) for each shotline.

7. Error File—The error file contains warnings and errors output by UEDDAM.

8. Debugging File—The debugging file contains all the temporary files generated by UEDDAM during a run. This file was intended to be used only for troubleshooting.

Because of the number of individual runs required to complete a performance run, only the hazard summary and hit summary files are output in these cases. The other output files are useful in troubleshooting and for closer inspection of specific cases.

Each individual run will result in a hazard and hit summary file. Each of the hazard summary files contains a P_{haz} for that combination of rotor, flight phase, engine, and debris type. At the end of each hazard summary is the average P_{haz} over a 360º sweep of release angles for each flight phase. A flight phase failure distribution weighted average of the flight phase P_{haz} was calculated for each run resulting in the average P_{haz} for a given rotor and debris type over a full flight envelope. This was then averaged for each engine, and finally, the two engine averages were combined to produce the aircraft 1-in-20 values.

The hit summary contains a list of components and multiply vulnerable groups (systems of redundant components), the average P_{haz} for each of those components or groups, and the SYSTEM P_{haz} for each run. The P_{haz} for each component or group is referred to as the component contribution to the SYSTEM P_{haz}. The SYSTEM P_{haz} is the probability of catastrophic hazard for the run, the same as the P_{haz} over 360º release that is reported in the hazard summary file. The sum of all of the component contributions to the P_{haz} can sometimes be greater than the SYSTEM P_{haz}. This difference occurs because UEDDAM uses the incremental method for determining P_{haz} along a shotline. This means that the P_{haz} along a shotline will not exceed 1.0 even if more than one critical component is intersected by that shotline. However, each of the critical components intersected by the shotline will be assigned a P_{haz}. So, if two or more critical components lie on the shotline, the sum component contributions may exceed the calculated SYSTEM P_{haz}.

For the purposes of this analysis (and to be consistent with AC 20-128A guidance), the component dysfunction, given a hit, for all components was 1.0. Therefore, the SYSTEM P_{haz} for that iteration will only be affected if that component was the only other critical component on that shotline. Therefore, it is important to look at both the system (overall) P_{HAZ} and component P_{haz} for each configuration.

3.5 INPUT AND OUTPUT FORMATTING.

In addition to UEDDAM, several other programs were used to reduce the user workload. Input and output formatting programs were created to automate the process of creating the UEDDAM control files and to collect the data from the various output files. These input and output programs were required due to the number of cases that needed to be executed for a production run. For the GBJ, three programs were used. The first program was an input generation program that created all the file structure and control files required for a production run as well as input decks for the output program. The second program was a batch file that was created by the input generation program to execute UEDDAM for each of the control files it created. The third program used an input deck created by the file generation program to open each output file and copy the probability of hazard for each combination of flight phase, debris category, engine, and rotor, and write it to a table. The values from the completed tables were then used to perform the 1-in-20 analysis, as specified in the AC 20-128A, appendix 1. A similar process was also used for the GT analysis.

4. ANALYSIS RESULTS.

The following section discusses the results of the UEDDAM analysis. Due to the increased size and complexity, fewer trade studies and investigations were performed on the GT than the GBJ.

4.1 GENERIC TWIN-ENGINE AIRCRAFT.

4.1.1 Analysis Results.

The results of the first analysis (called original) were presented at the 28th PPIHWG meeting. The participants recommended a series of modifications to the GT to highlight specific failure characteristics and better represent in-service aircraft. The primary changes in the model geometry were to lower the engines relative to the fuselage to address cross engine debris, and to modify the wing spar criticality to include the damage tolerance built into the wing spar and stringer structure. In addition to aircraft modifications, the PPIHWG participants recommended a change in the debris categories assessed and the resulting analysis was referred to as the updated baseline analysis. A comparison by debris type of the 1-in-20 results for the original and baseline analyses can be seen in figure 4-1.

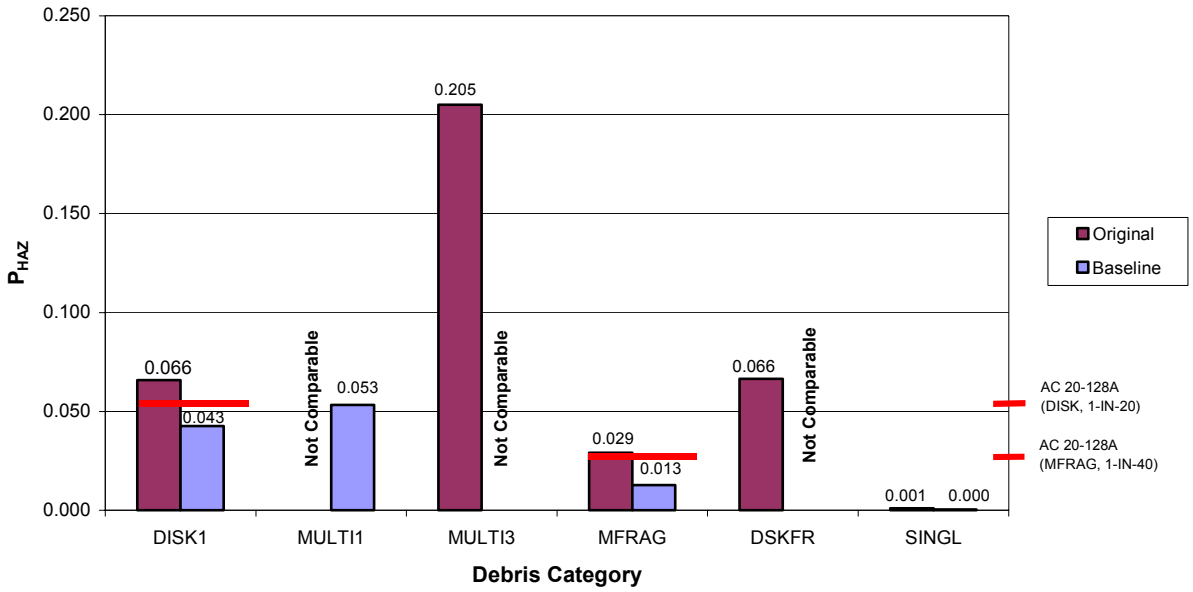

FIGURE 4-1. COMPARISON OF OVERALL AVERAGES BETWEEN ORIGINAL AND BASELINE RESULTS

Note that for both the DISK1 and MFRAG debris categories, the original overall averages exceed the AC 20-128A criteria for acceptable risk levels for similar debris types (see table 4-1), shown as red lines in figure 4-1. After modifications were made to the generic twin engine aircraft, the baseline overall averages of the aforementioned debris categories decreased to below the acceptable risk level. The specific reason for this reduction is discussed further on.

TABLE 4-1. SUMMARY OF ACCEPTABLE RISK LEVEL CRITERIA
(Extraction of table 1, AC 20-128A)

Requirement	Criteria
Average 1/3 Disk Fragment	1 in 20 (0.050)
Average Intermediate Fragment	1 in 40 (0.025)
Average Alternate Model	1 in 20 @ ±5° Spread Angle (0.050)
Multiple Disk Fragments	1 in 10 (0.100)
Any Single Fragment (Except for Structural Damage)	2 × corresponding average criterion

Figures 4-2 through 4-13 provide additional details of the results organized by debris category—the odd numbered figures show the results by engine section (averaged over both engines), whereas the even numbered figures show the main contributors to catastrophic damage (averaged over all engine sections and both engines). It is important to note that for the debris categories DISK1, MFRAG, DSKFR, and MULTI3 (see figures 4-2, 4-4, 4-8, and 4-10), the turbine section of the engine contributes the most to the overall probability of catastrophic damage in the original analysis due to the location of the turbine section with respect to the leading-edge spar. The debris zone of the turbine section intersects the wing leading-edge spar (the original analysis had the wing leading-edge spar as critical and singularly vulnerable). This also explains the dramatic drop in the turbine section contribution between the original and baseline results for the DISK1 and MFRAG debris categories. The increased redundancy of the wing structure greatly reduces the impact of the turbine section debris. For the debris categories SINGL and MULTI1, it is the fan section that makes the largest contribution (see figures 4-5 and 4-11). In fact, for both the original and the baseline analyses, the only significant contributor to SINGL debris damage is from the fan section. This is because the fan section is the only section that can produce a large enough fragment to defeat critical components.

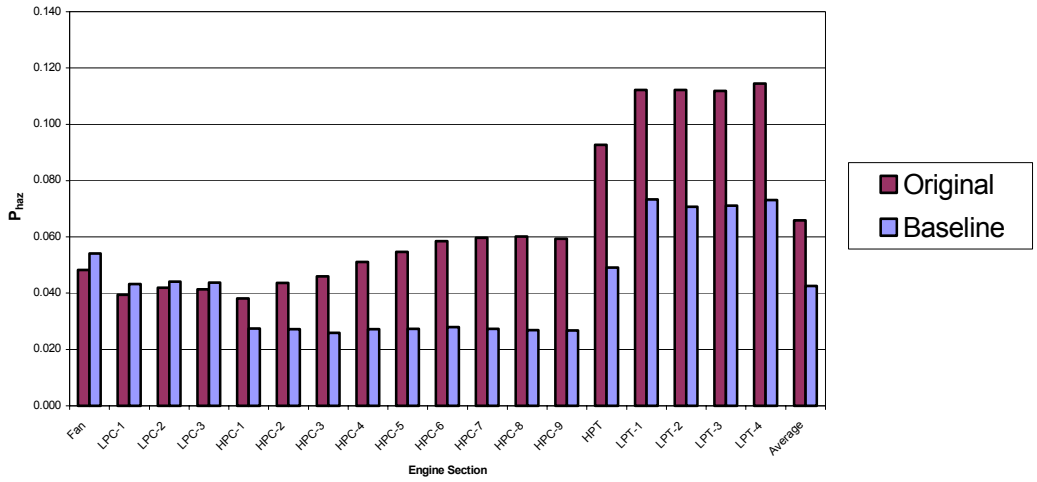

FIGURE 4-2. COMPARISON BETWEEN ORIGINAL AND BASELINE RESULTS BY ENGINE SECTION FOR DISK1

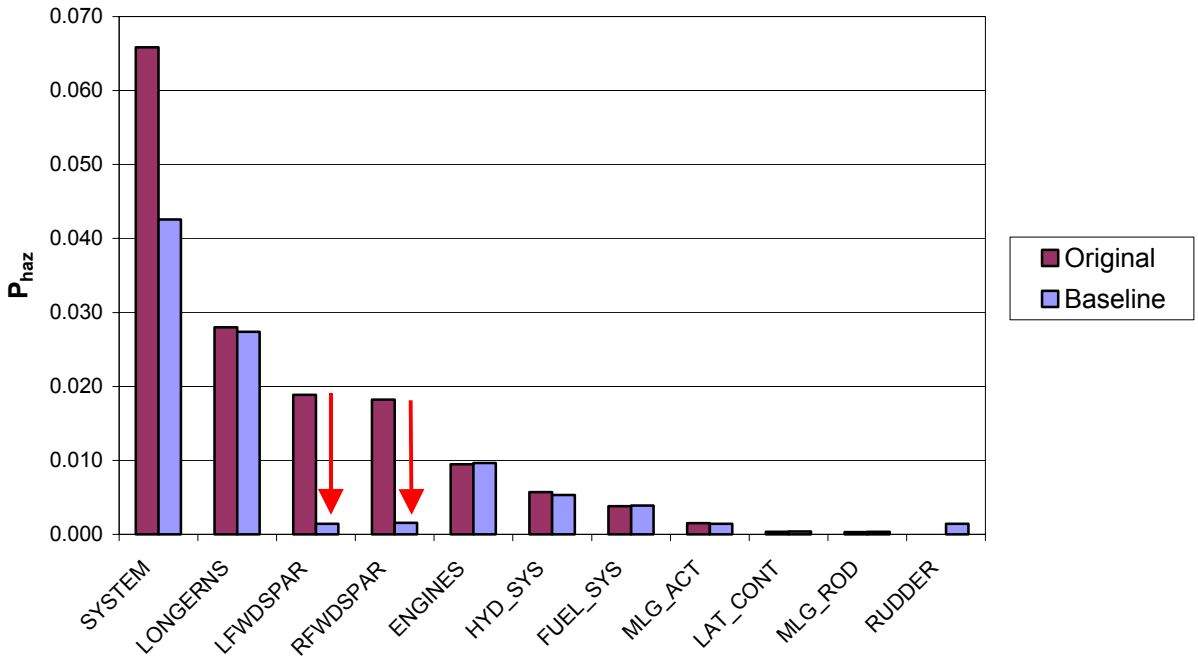

FIGURE 4-3. SYSTEM CONTRIBUTION COMPARISON BETWEEN ORIGINAL AND BASELINE RESULTS FOR DISK1

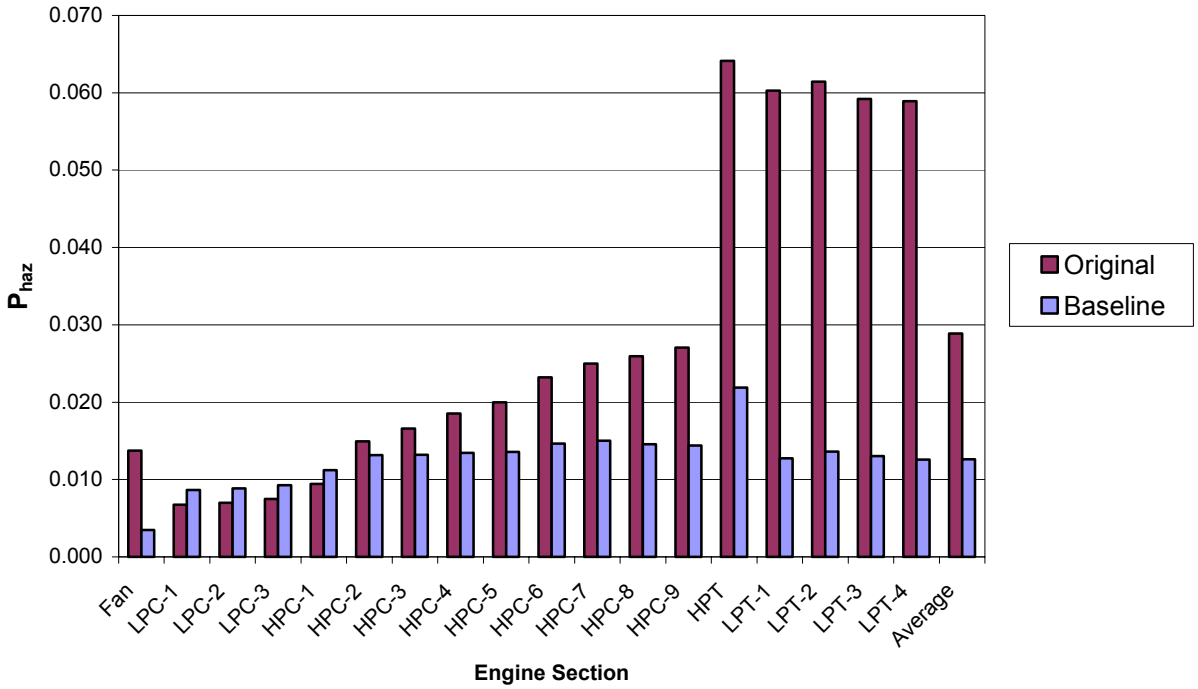

FIGURE 4-4. COMPARISON BETWEEN ORIGINAL AND BASELINE RESULTS BY ENGINE SECTION FOR MFRAG

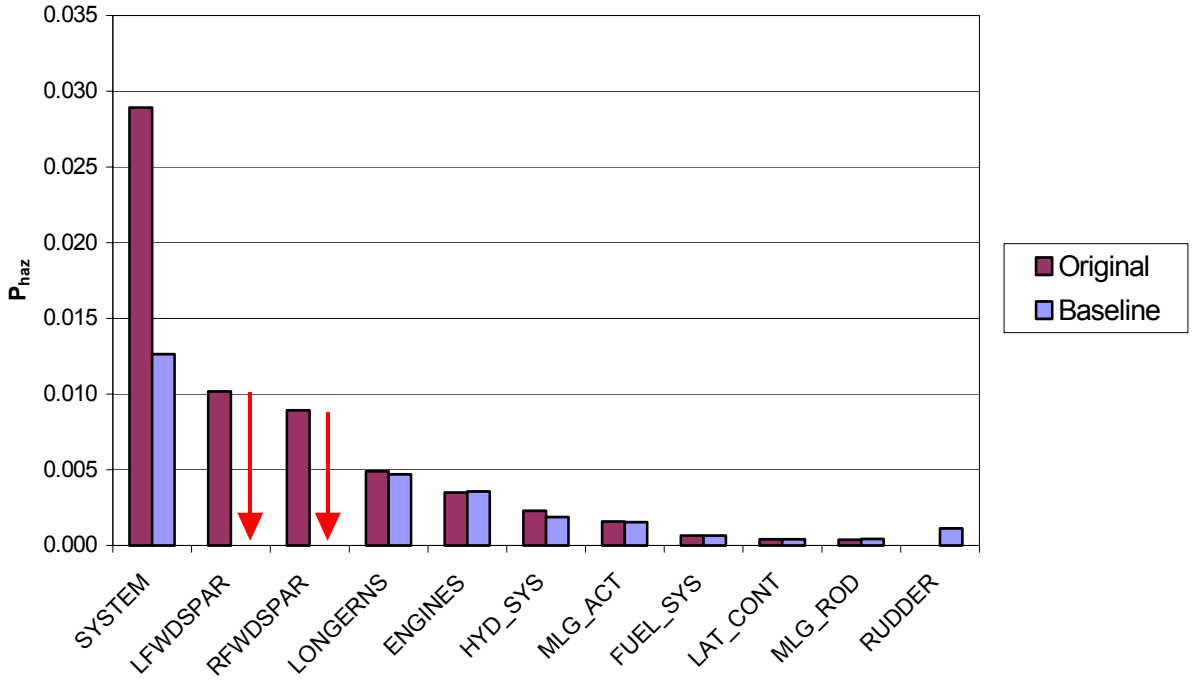

FIGURE 4-5. SYSTEM CONTRIBUTION COMPARISON BETWEEN ORIGINAL AND BASELINE RESULTS FOR MFRAG

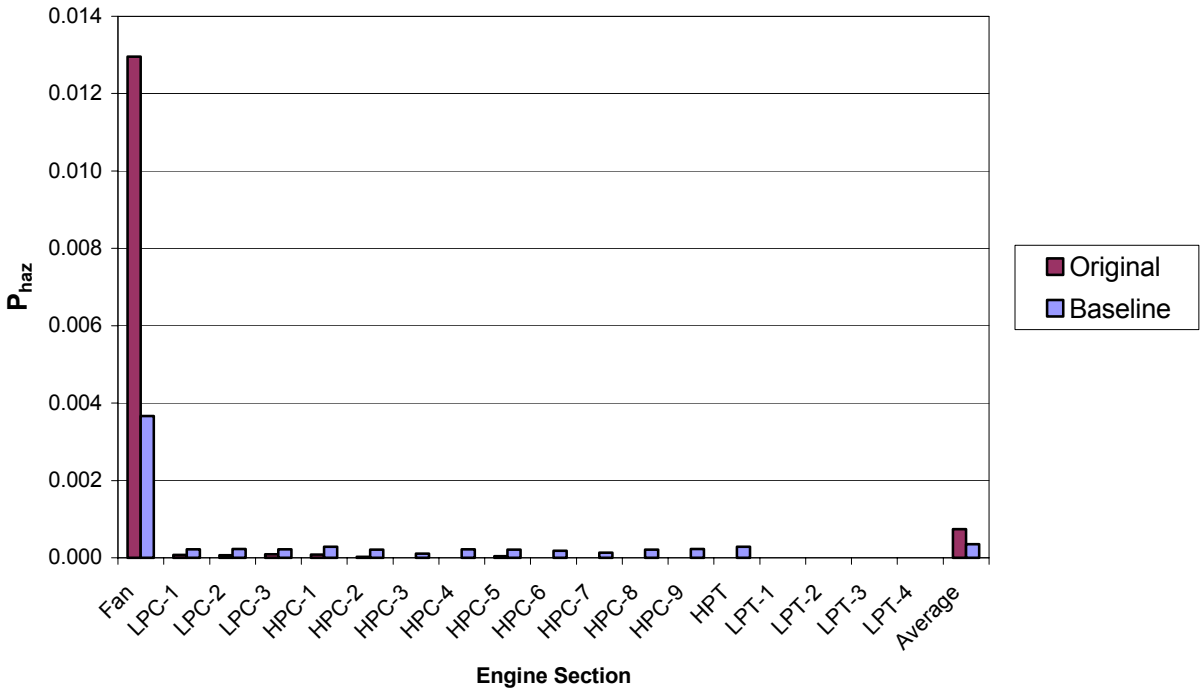

FIGURE 4-6. COMPARISON BETWEEN ORIGINAL AND BASELINE RESULTS BY ENGINE SECTION FOR SINGL

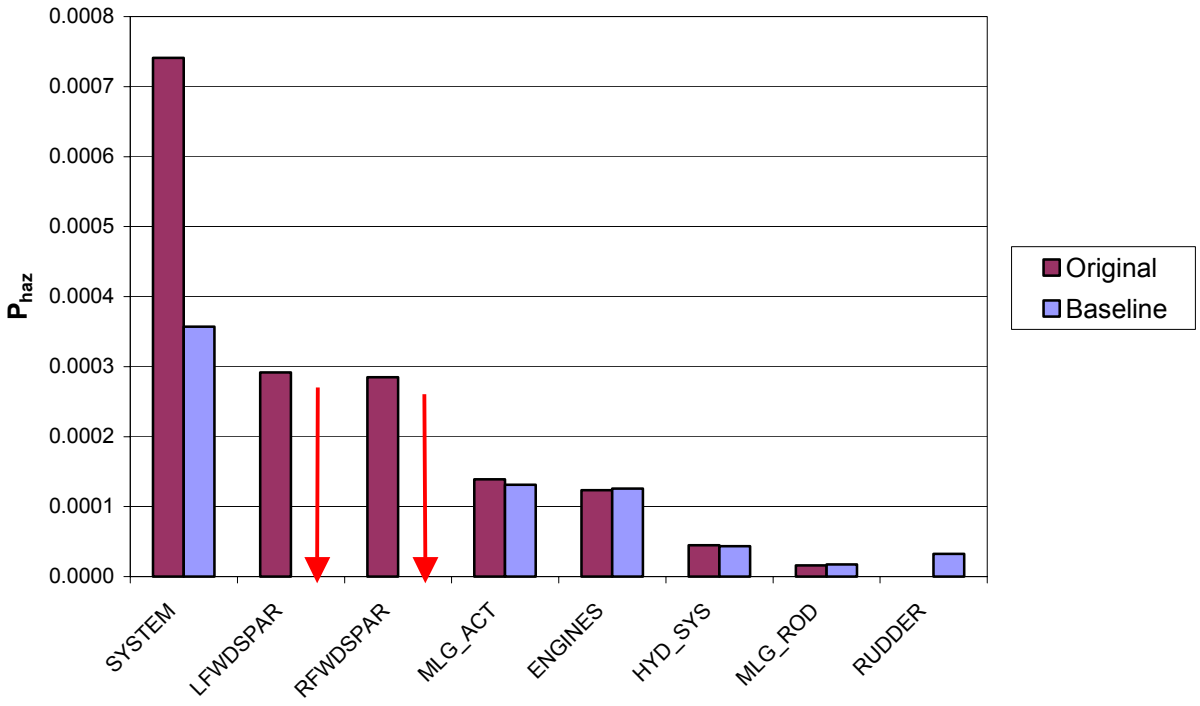

FIGURE 4-7. SYSTEM CONTRIBUTION COMPARISON BETWEEN ORIGINAL AND BASELINE RESULTS FOR SINGL

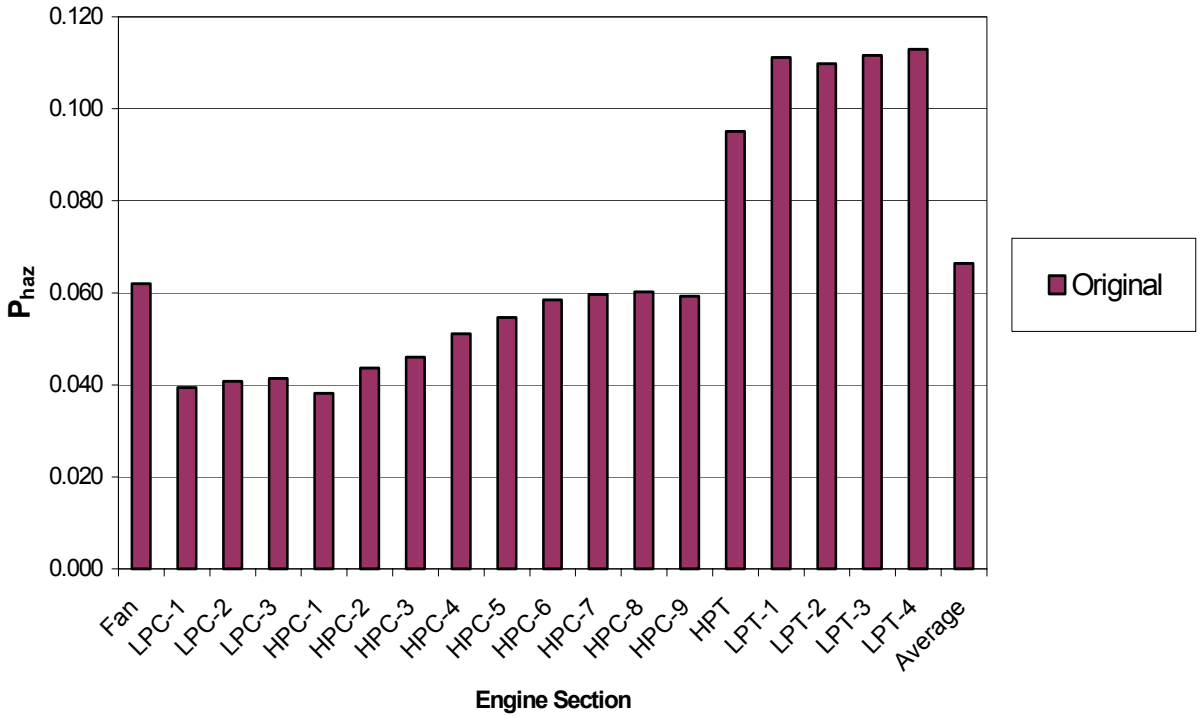

FIGURE 4-8. ORIGINAL RESULTS BY ENGINE SECTION FOR DSKFR

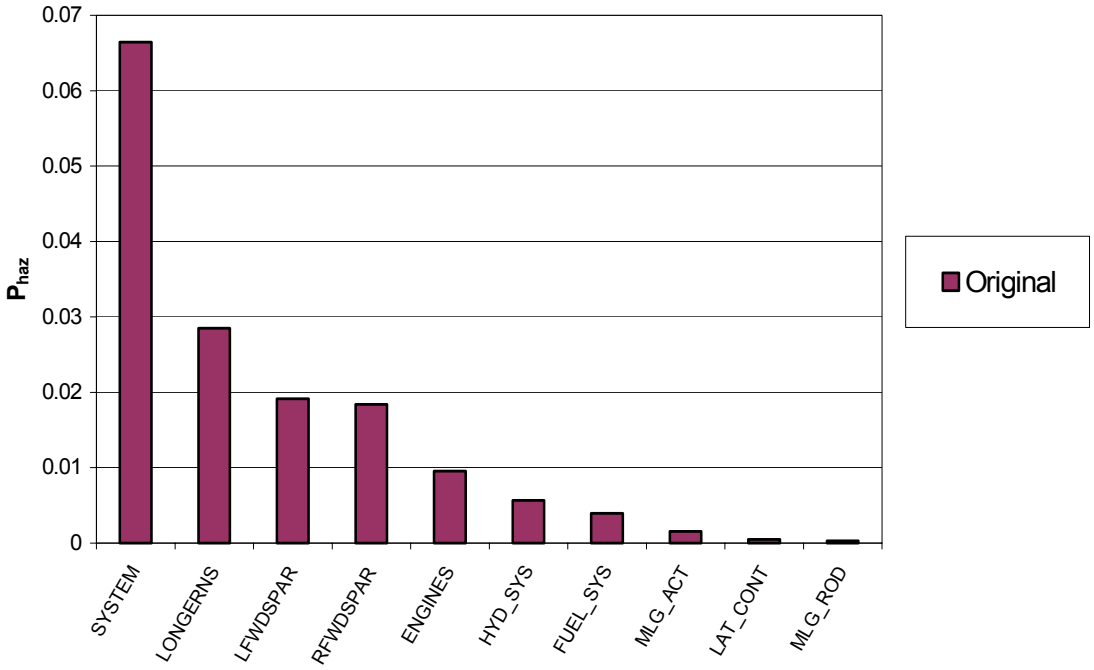

FIGURE 4-9. ORIGINAL SYSTEM CONTRIBUTION RESULTS FOR DSKFR

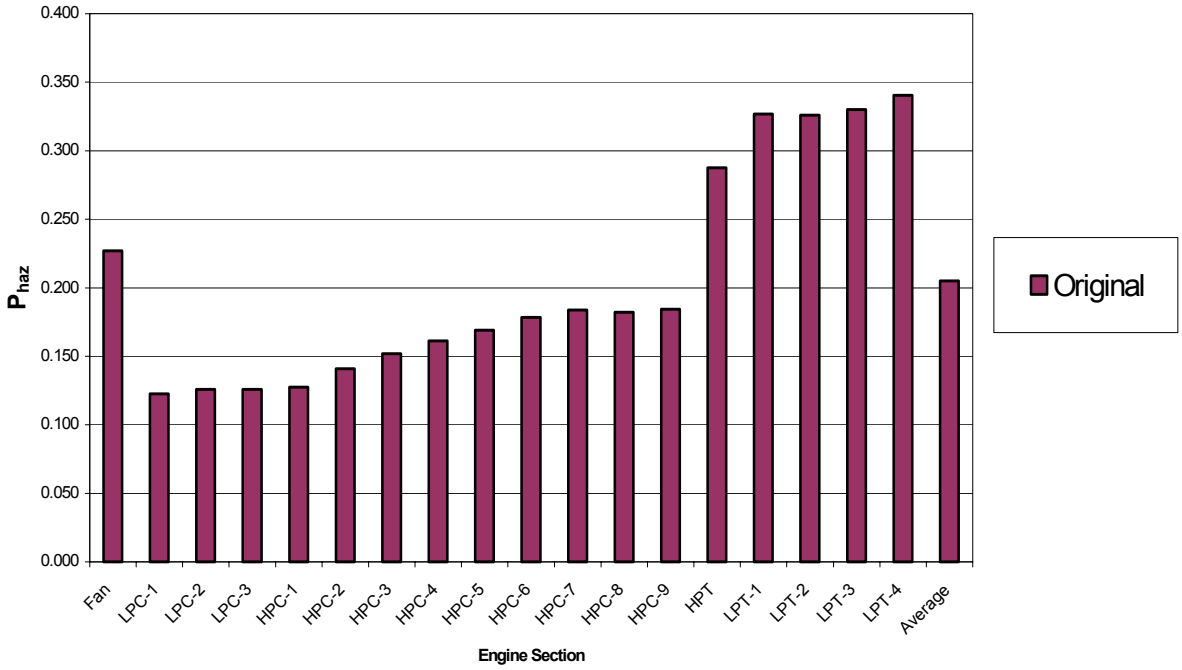

FIGURE 4-10. ORIGINAL RESULTS BY ENGINE SECTION FOR MULTI3

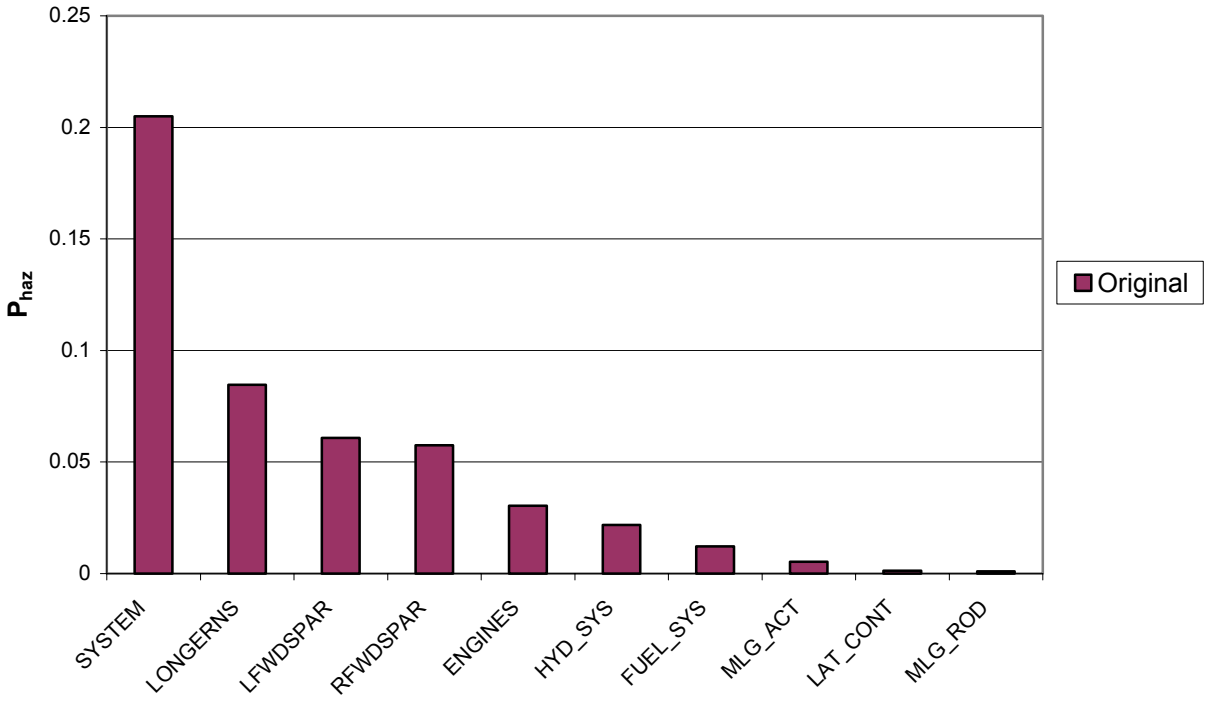

FIGURE 4-11. ORIGINAL SYSTEM CONTRIBUTION RESULTS FOR MULTI3

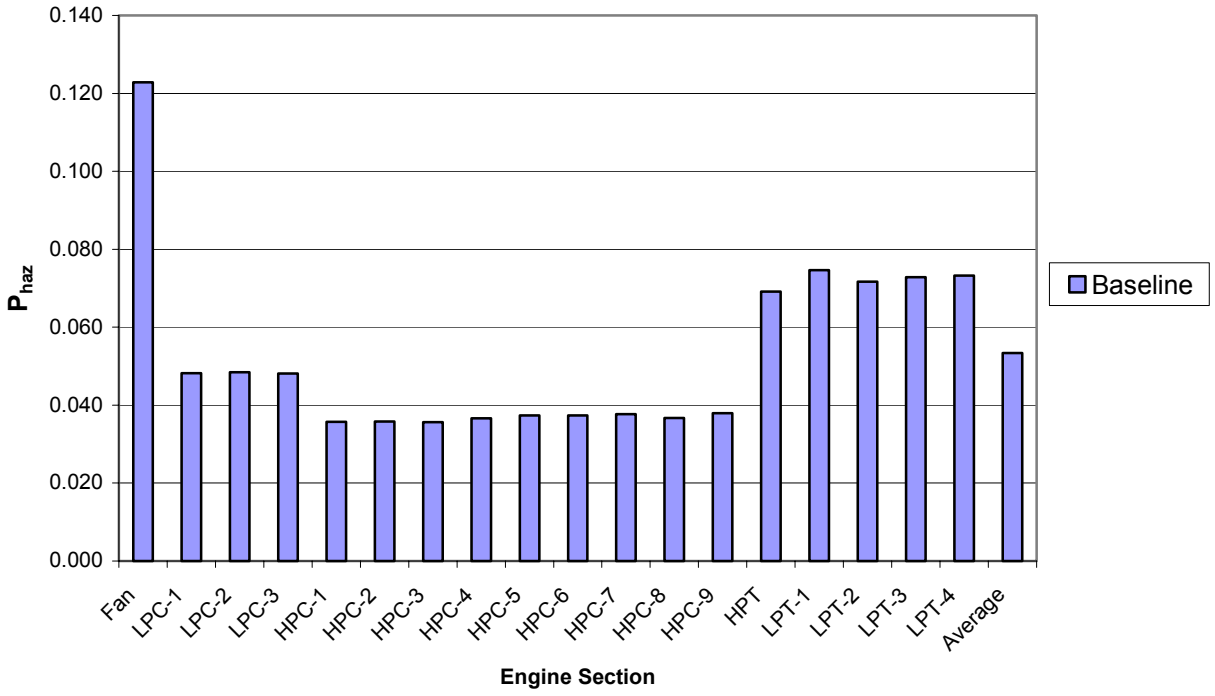

FIGURE 4-12. BASELINE RESULTS BY ENGINE SECTION FOR MULTI1

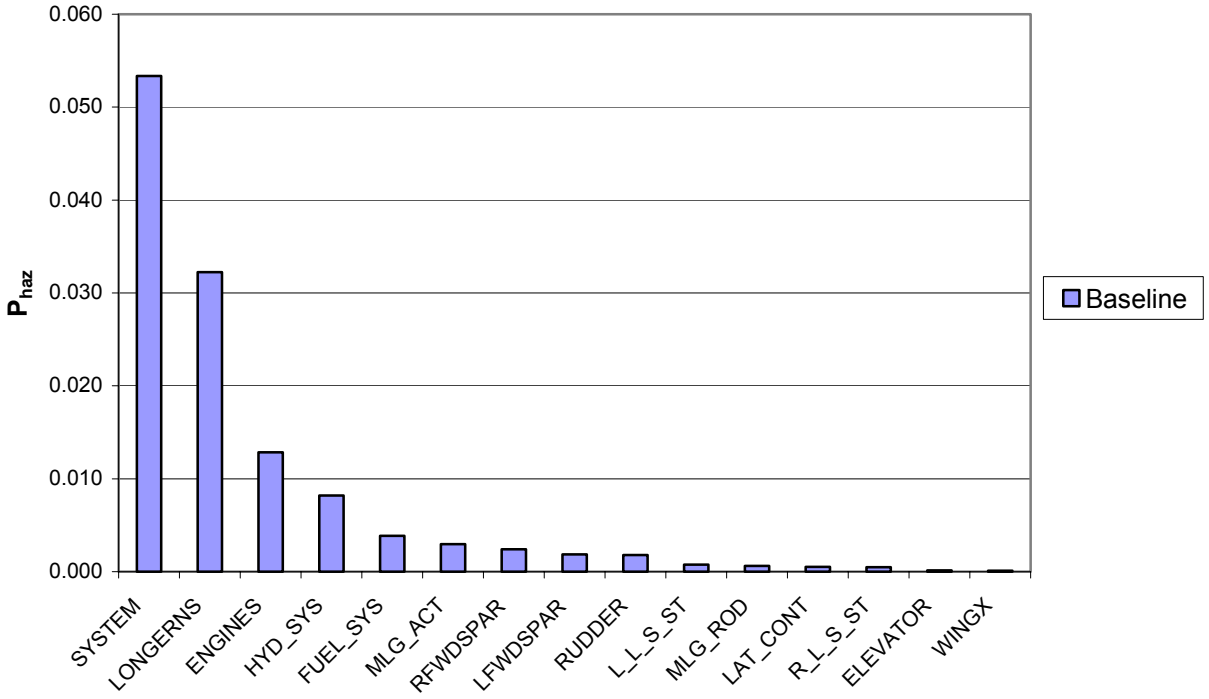

FIGURE 4-13. BASELINE SYSTEM CONTRIBUTION RESULTS FOR MULTI1

For the three comparable debris categories (DISK1, MFRAG, and SINGL), the decline from the original to the baseline results can be explained by the change in wing spar criticality (see figures 4-2, 4-4, and 4-6). In the original analysis, the left and right forward spars were defeated when a large fragment penetrated either the leading-edge or trailing-edge spar web. In the baseline analysis, however, for the left and right forward spars to be defeated, not only would the spar web have to be penetrated, but the top and bottom spar caps as well. In addition, certain combinations of failures of upper and lower stringers could cause catastrophic damage. Thus, by increasing the redundancy of the wing spar (and thereby changing its criticality), the overall probability of catastrophic damage was reduced.

Note also from figures 4-2, 4-4, and 4-6 that the rudder shows an increase in contribution to catastrophic damage. This is due to the fact that for the baseline condition, the loss of primary rudder control alone on takeoff would be sufficient to result in catastrophic damage whereas in the original analysis, it was assumed that, on takeoff, a loss of both primary and trim rudder control would be required for a catastrophic event. Also note that even though the wing fuel tanks became critical in the baseline analysis, no change resulted in their contribution. This results from the engines being far enough forward of the wing fuel tanks that the debris misses the tanks in almost all cases. Also, the impact of any potential hits on the wing fuel tanks are further diminished by the phase failure distribution of the descent phase (3%).

In addition to the modifications from the original configuration to the baseline configuration, a parametric study (referred to as the alternate analysis) in which the engines were lowered from the baseline configuration such that the engine centerline was level with the bottom of the

aircraft skin was performed to address cross engine debris under the fuselage. This adjustment was made to achieve a GT that represents a broader group of in-service aircraft. A comparison by debris category of the results from the baseline and alternate analyses can be seen in figure 4-14.

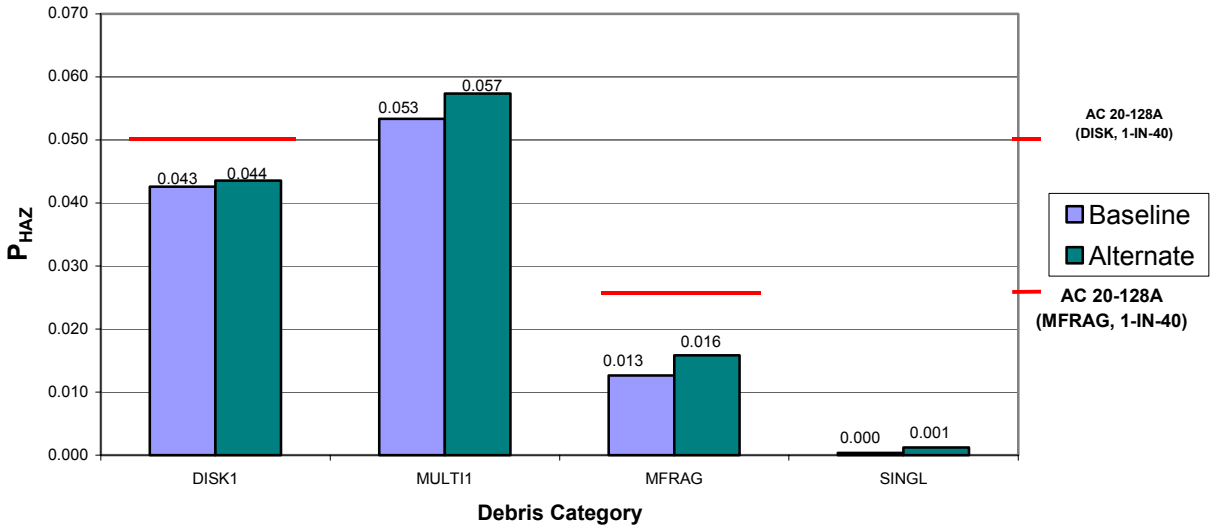

FIGURE 4-14. COMPARISON OF OVERALL AVERAGES BETWEEN BASELINE AND ALTERNATE RESULTS

The red lines in figure 4-14 again represent the AC 20-128A levels of maximum allowable probability of catastrophic hazard (see table 4-1) for the debris categories DISK1 and MFRAG. Note that lowering the engines increases the overall probability of catastrophic damage for each debris category assessed, but not enough to raise the probabilities to an unacceptable risk level.

As before, figures 4-15 through 4-22 provide further details of the results organized by debris category; the even figures show the results by engine section (averaged over both engines), whereas the odd figures show the main contributors to catastrophic damage (averaged over all engine sections and both engines). Since all debris categories assessed were identical, the results for the baseline and alternate analyses are always displayed on the same graph. It is important to note that for the debris categories DISK1 and MFRAG, the turbine section of the engine (specifically, the low-pressure turbine for DISK1 and the high-pressure turbine for MFRAG) contributes the most to the overall probability of catastrophic damage. For the DISK1 debris categories, the low-pressure turbine section debris is large enough to defeat the leading-edge spar in some cases. For the MFRAG debris category (and the DISK1), the high-pressure turbine section debris has enough size and energy to defeat redundant structure. For the debris categories SINGL and MULTI1, it is the fan section that makes the largest contribution (see figures 4-14, 4-16, 4-18, and 4-20). However, contrary to the original and baseline analyses, in the alternate analysis, the fan section is not the only significant contributor to SINGL debris damage—the compressor section (including both the high- and low-pressure sections) and the high-pressure turbine play a nontrivial part as well, due to the cross-engine debris effects.

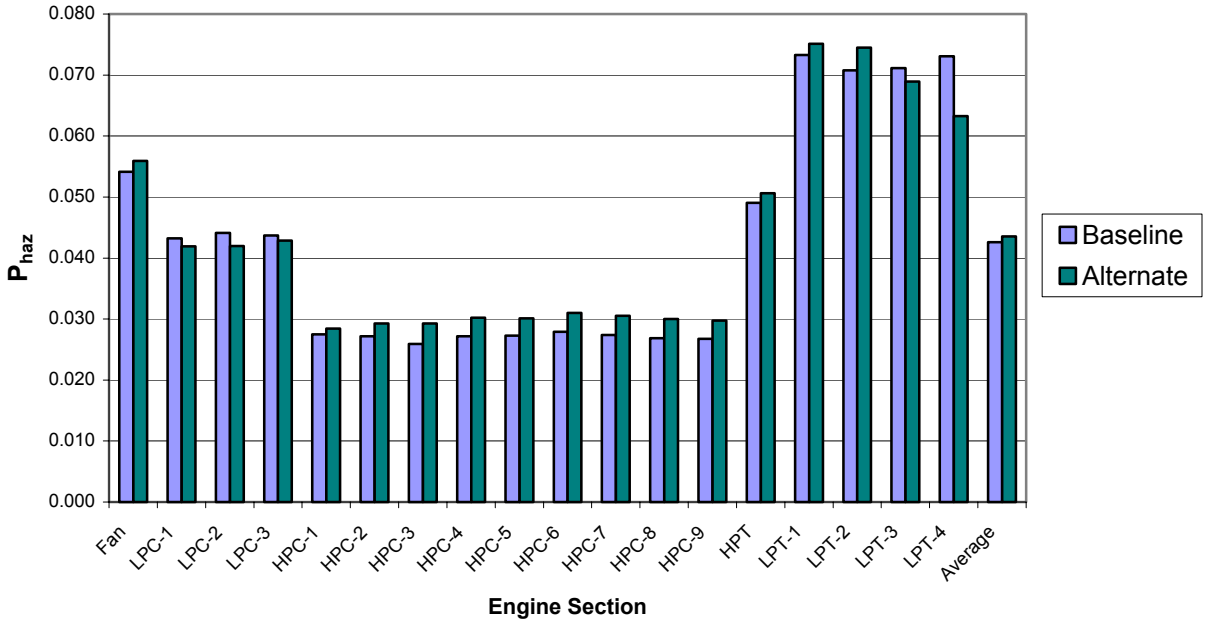

FIGURE 4-15. COMPARISON BETWEEN BASELINE AND ALTERNATE RESULTS BY ENGINE SECTION FOR DISK1

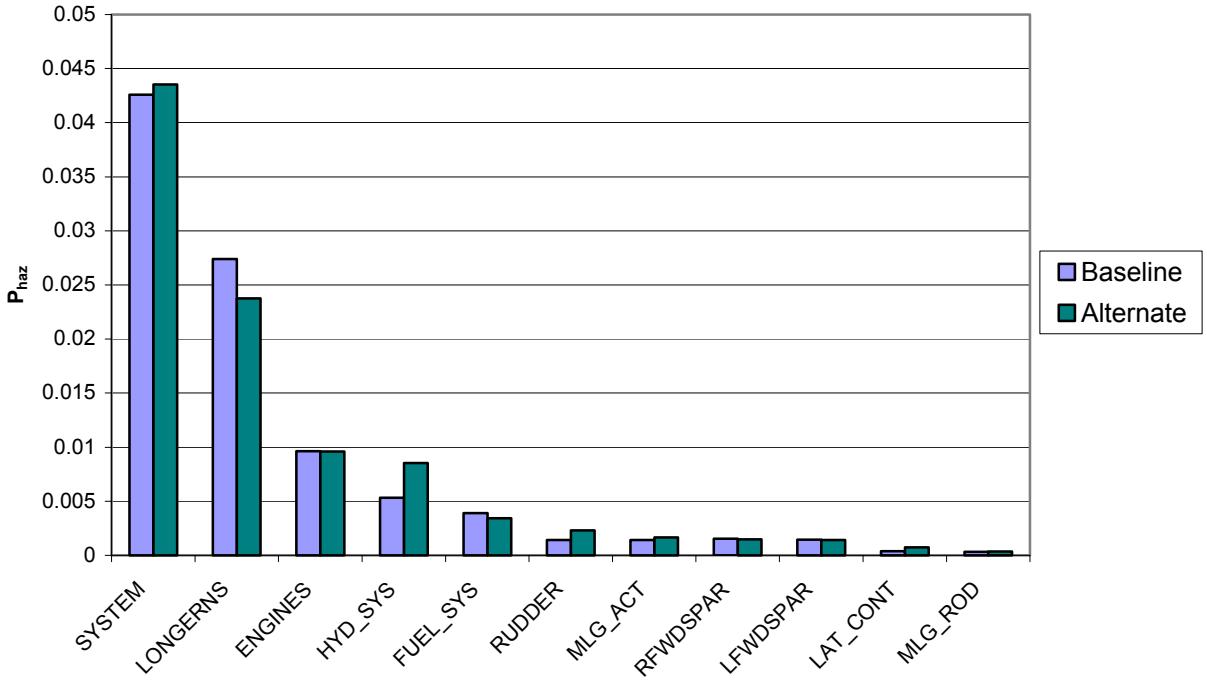

FIGURE 4-16. SYSTEM CONTRIBUTION COMPARISON BETWEEN BASELINE AND ALTERNATE RESULTS FOR DISK1

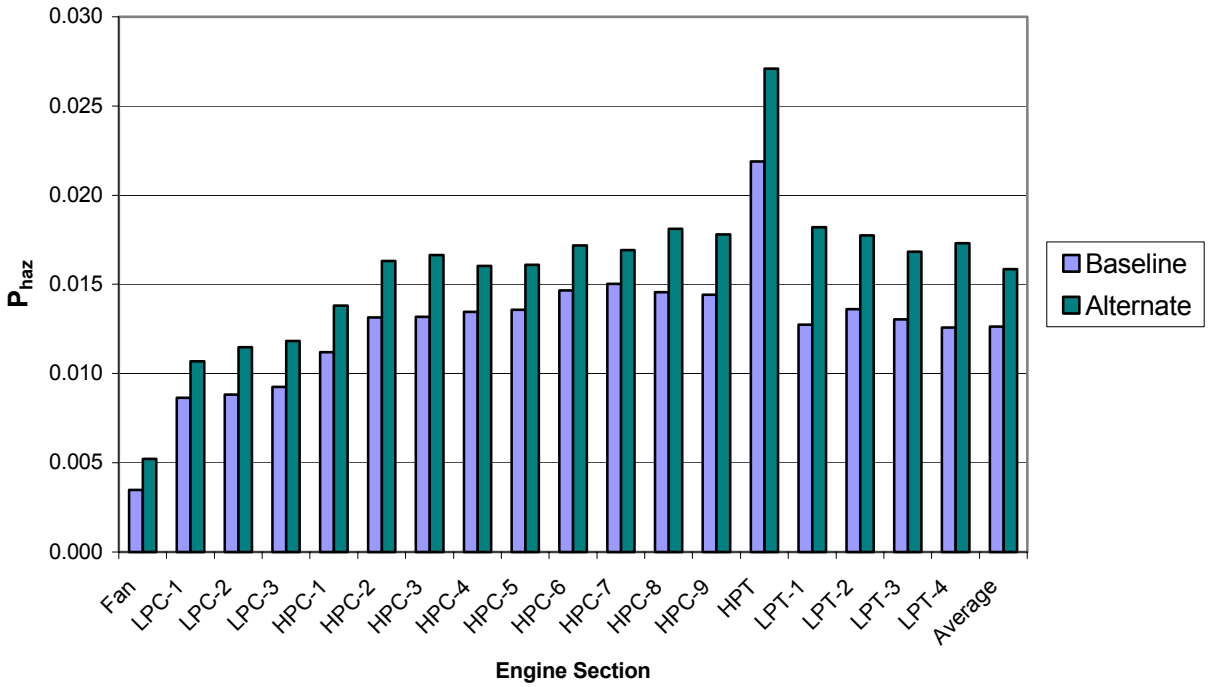

FIGURE 4-17. COMPARISON BETWEEN BASELINE AND ALTERNATE RESULTS BY ENGINE SECTION FOR MFRAG

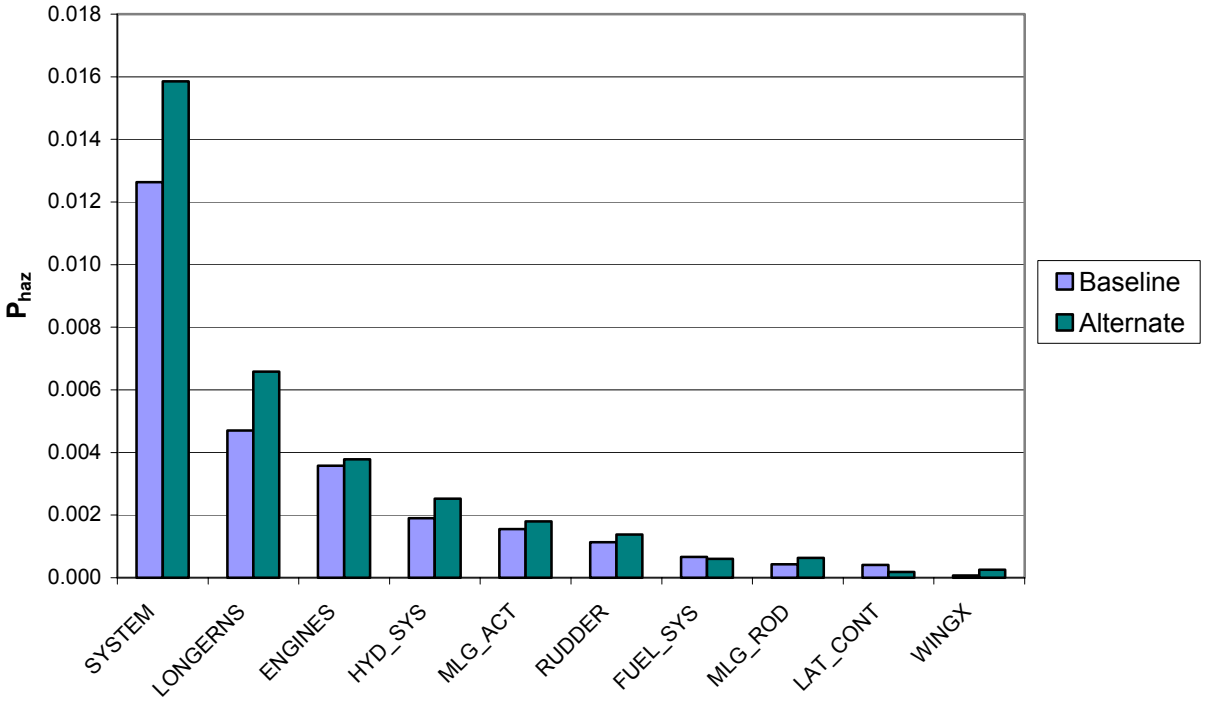

FIGURE 4-18. SYSTEM CONTRIBUTION COMPARISON BETWEEN BASELINE AND ALTERNATE RESULTS FOR MFRAG

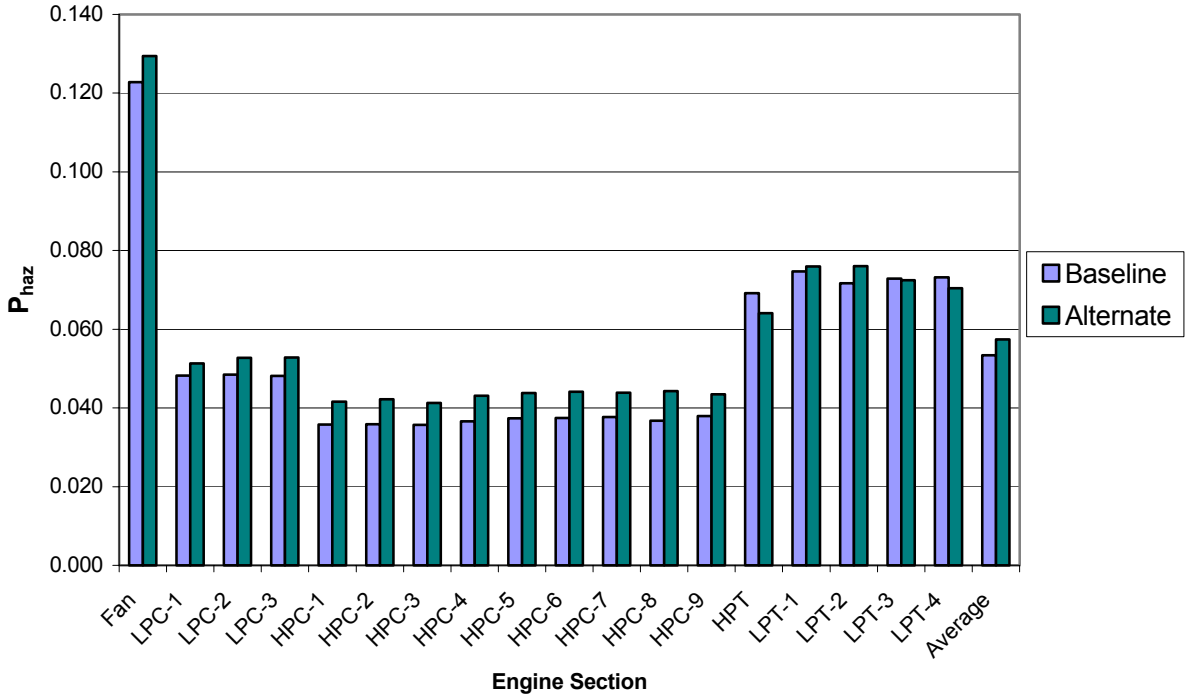

FIGURE 4-19. COMPARISON BETWEEN BASELINE AND ALTERNATE RESULTS BY ENGINE SECTION FOR MULTI1

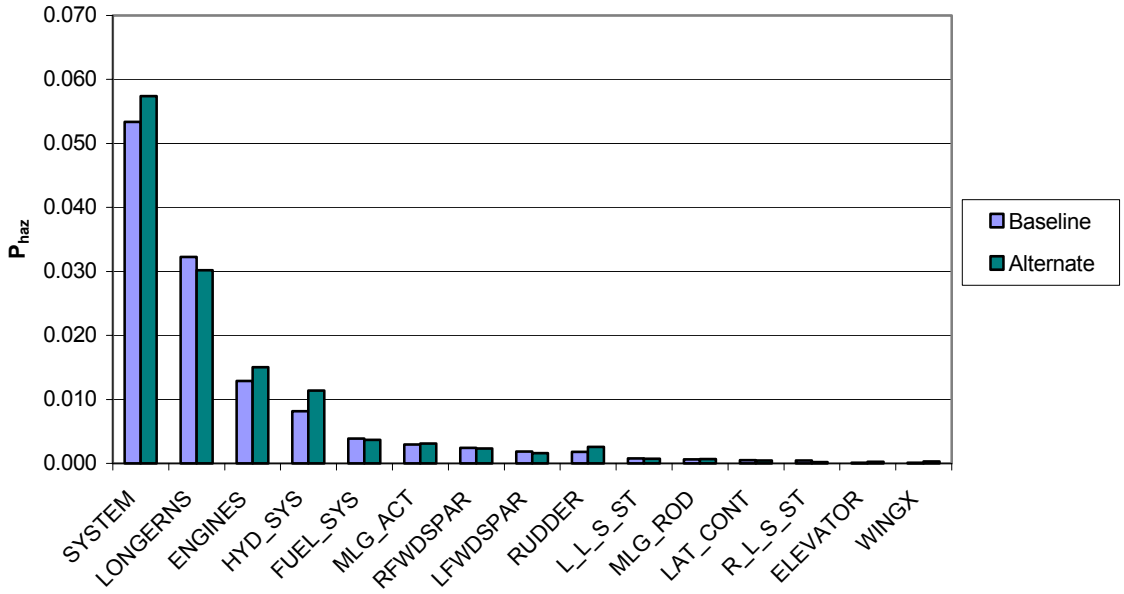

FIGURE 4-20. SYSTEM CONTRIBUTION COMPARISON BETWEEN BASELINE AND ALTERNATE RESULTS FOR MULTI1

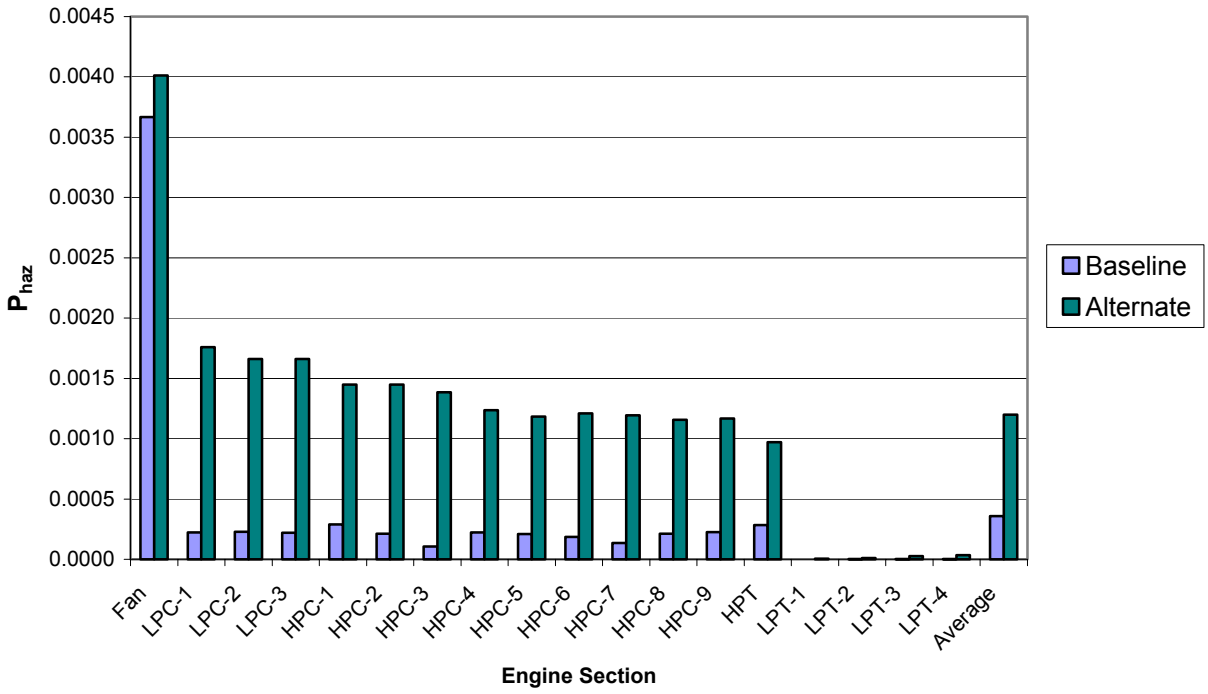

FIGURE 4-21. COMPARISON BETWEEN BASELINE AND ALTERNATE RESULTS BY ENGINE SECTION FOR SINGL

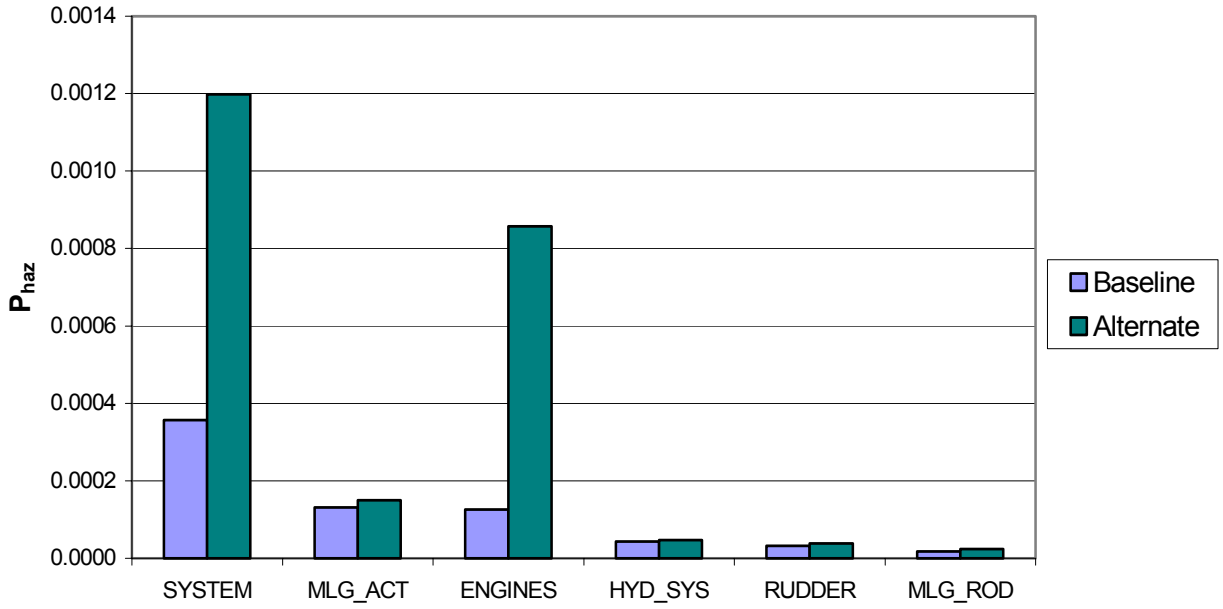

FIGURE 4-22. SYSTEM CONTRIBUTION COMPARISON BETWEEN BASELINE AND ALTERNATE RESULTS FOR SINGL

Figures 4-16, 4-18, 4-20, and 4-22 show the baseline and alternate system contributions to catastrophic damage for the DISK1, MFRAG, MULTI, and SINGL debris categories. The DISK1, MFRAG, and MULTI system contributions are very similar. Specifically, the top three contributors for all three debris types are the LONGERNS (defeat of five adjacent fuselage structural longerons), ENGINES (defeat of opposite engine via cross engine debris), and HYD_SYS (defeat of redundant components in the hydraulic systems). With LONGERNS being the leading contributor to catastrophic damage, a thorough investigation of this assumption is warranted. The results indicate that for the larger debris fragments, the aircraft fuselage structural defeat is a major issue. Note that this contribution is based on the assumption that defeat of five adjacent fuselage structural longerons would result in catastrophic damage in all flight modes. The second leading contributor for the DISK1, MFRAG, and MULTI debris categories is the defeat of the opposite engine via cross engine debris. The contribution of ENGINES changes little from the baseline to the alternate aircraft configuration because the larger fragments have sufficient energy to penetrate through fuselage and damage opposite engine. The hydraulics system (HYD_SYS) was the third highest contributor to P_{HAZ}. This indicates that the arrangements of the hydraulic system components align with respect to some of the debris trajectories. For the SINGL debris category (see figure 4-22) the leading contributors are the MLG_ACT (critical elements of the main landing gear actuator), ENGINES, and HYD-SYS. For the alternate configuration, the ENGINES become the leading contributor revealing the sensitivity of cross engine defeat based on engine location for the small fragments.

The increase from the baseline to the alternate results is manifested as increases in different system contributions, depending on the debris category considered (see figures 4-16, 4-18, 4-20, and 4-22). For instance, when considering the debris category MFRAG, increases in every system (excluding the fuel and lateral flight control systems) contribute to the overall increase in P_{HAZ} from baseline to alternate results. The debris category DISK1, on the other hand, shows a primary increase in contribution from the hydraulic system, but is offset by a decrease in the fuselage structure contribution from baseline to alternate results. Similarly, the MULTI1 debris category follows the DISK1 trend with the exception that the small fragments released in the MULTI1 case additionally increase the cross engine defeat probability (ENGINES) for the alternate configuration. Lastly, for the debris category SINGL, the overall probability of catastrophic damage increase is concentrated in a nearly eight-fold increase in the engine system's contribution, which is a direct result of exposing the engines to cross-engine debris. The reason that there is not a dramatic increase for the other debris types is that the other debris types have enough energy to penetrate through the aircraft body and defeat the other engine in the baseline configuration, whereas the SINGL debris does not. Exposing the opposite engine has little impact for the other debris types, but allows the smaller and lower energy fragments of the SINGL debris category to reach and damage the opposite engine. The turbine blades (in the SINGL debris category) do not contribute much to the overall P_{HAZ} of the system for several reasons (see figure 4-21). This is primarily because the relatively small size and energy of the turbine blade fragments. Also, the turbines are located in the aft section of the engine and the aft spread angle tends to be further aft than other sections increasing the likelihood of the fragments missing the opposite engine.

4.1.2 Sensitivity Study.

The purpose of the sensitivity study was to assess the responsiveness of the P_{HAZ} to an increase in engine nacelle thickness using UEDDAM. The study was performed with the alternate geometric configuration and took into consideration three debris categories (MULTI1, DISK1, and SINGL). The nacelle thickness considered in this study were selected by estimating the thickness of aluminum required to stop all the large and small fragments making up the debris categories MULTI1 and SINGL and applying these skin thicknesses to the areas indicated in red in figure 4-23. The equation used in estimating these thicknesses was the COVART fragment penetration equation, which is founded on FAA equations that have been modified by China Lake (based on engine debris penetration testing). For example, using the fragment penetration model, the residual velocity of the large fan fragment in the debris category MULTI1 can be found to be equal to zero after it penetrates a 0.48″ aluminum plate. Thus, in addition to the original 0.04″ thickness, the sensitivity study included both the upper and lower limits of 1.1″ (corresponding to the large HPT fragment) and 0.12″ (corresponding to the small LPT fragment) as well as a midpoint thickness of 0.48″.

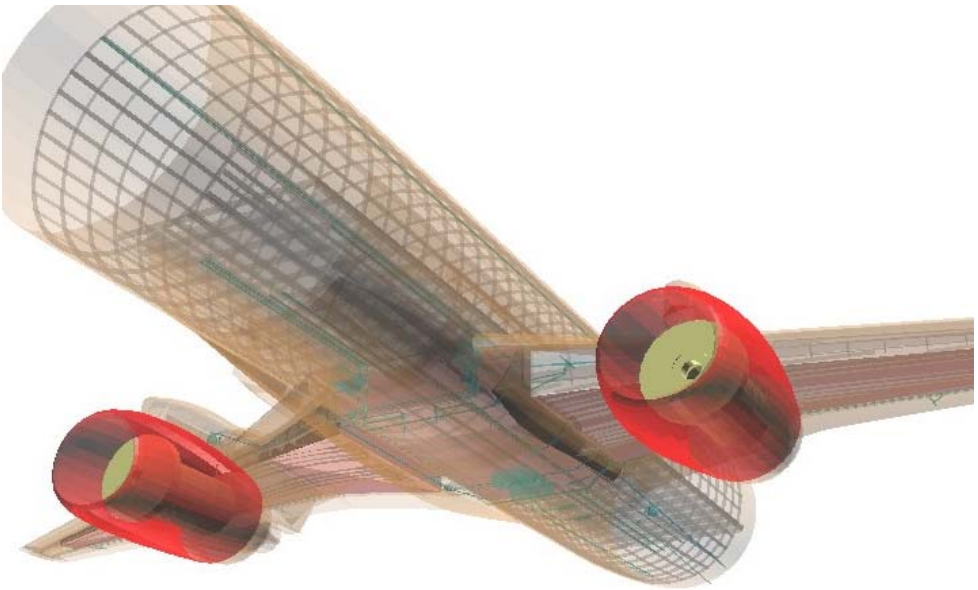

FIGURE 4-23. ALTERNATE GEOMETRIC CONFIGURATION WITH ENGINE NACELLES HIGHLIGHTED IN RED

4.1.3 Analysis.

A summary of the results of the sensitivity study can be seen in figure 4-24. As expected, by increasing the engine nacelle thickness, the probability of catastrophic damage is reduced, but the decrease does not occur in a linear fashion. An increase 0.09″ from the original 0.04″ thick aluminum was seen to have a limited effect in reducing the probability of catastrophic damage due to MULTI1, however, the increase in nacelle thickness to 0.48″ reduces the P_{HAZ} to 0.6%, well below the AC 20-128A 1-in-20 requirement for a single 1/3 disk segment (see table 4-1). Although the MULTI1 debris category contains multiple fragments in addition to a disk segment,

this analysis shows that the GT can meet a 1-in-20 requirement to a more damaging debris field. Because the effects of increasing the skin thickness are nonlinear, more data points between these two nacelle thickness should be performed for a better evaluation of the optimum nacelle thickness to reduce damage from larger fragments.

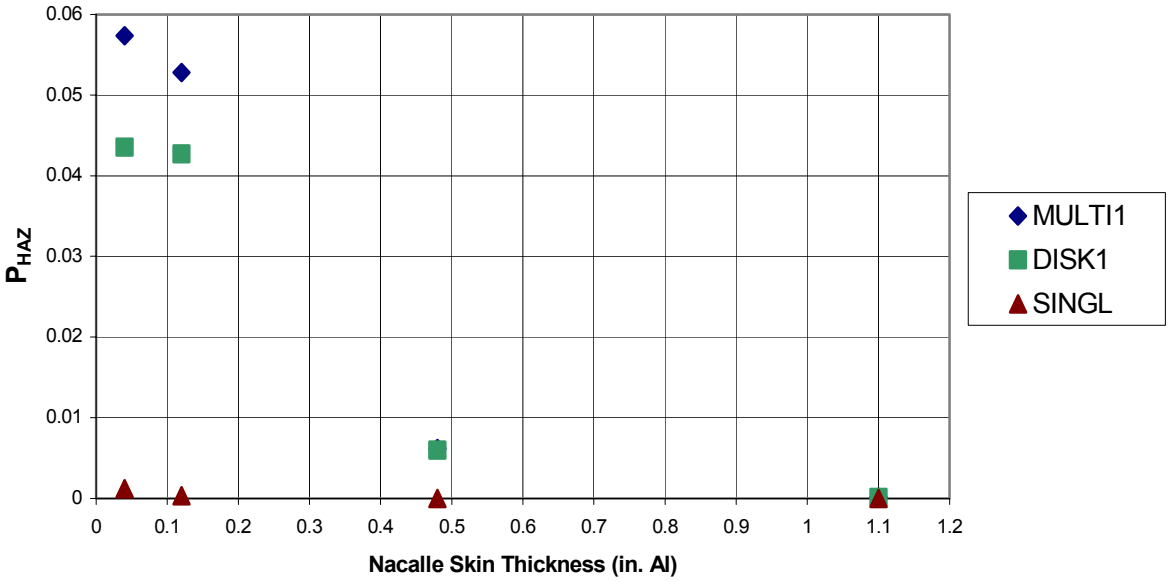

FIGURE 4-24. PROBABILITY OF CATASTROPHIC DAMAGE (P_{HAZ}) VS NACELLE SKIN THICKNESS FOR THREE DEBRIS TYPES

One notable result was seen for the HPT section of the 1.1″ nacelle thickness case. The DISK1 probabilities for catastrophic damage for the HPTs of engines 1 and 2 were equal to zero, but the same probabilities for the debris category MULTI1 were slightly greater than zero. At first this appears counterintuitive because the only difference between the two debris types is the addition of small fragments, which should not be able to perforate the 1.1″ engine nacelle. However, upon closer inspection, it was determined that the HPT hazard zone for the debris category MULTI1 (highlighted in blue in figure 4-25) extends beyond the aft end of the engine nacelle and therefore, the shotlines for some of the small fragments were not shielded by the thickened nacelle skin. Note that had the SINGL UEDDAM runs been performed for the 0.48″ and 1.1″ thicknesses, the same phenomenon would have been noticed since the fore and aft spread angles for the HPT small fragments are the same (+15º and -60º) in both the SINGL and MULTI1 debris categories; however, because the values for the SINGL debris case are almost an order of magnitude smaller than those of the other debris categories, this phenomenon would be insignificant at the scale shown in figure 4-24.

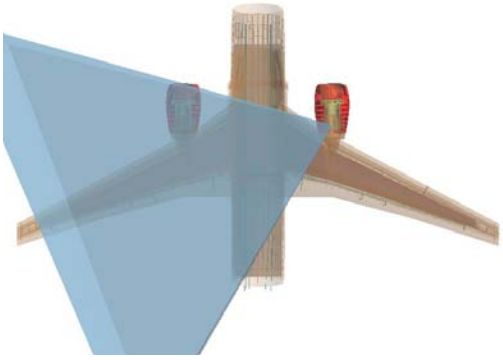

FIGURE 4-25. ENGINE 1 HPT HAZARD ZONE FOR THE DEBRIS TYPE MULTI1

As part of the analysis, a rough estimate of the weight of shielding (i.e., the portion of the engine nacelles that would be thickened) required to protect the critical components of the aircraft from all of the debris categories was calculated. To do this, it was assumed that the engine nacelle could be modeled as a cylinder with a radius of approximately 38 inches and a uniform thickness.

These rough estimates assumed a single thickness of aluminum along the entire length of the engine nacelle. However, tailoring the nacelle thickness to each engine section and/or using more advanced materials (i.e., titanium, Kevlar, spectra, s-glass, etc.) could dramatically reduce the weights listed in table 4-2. For example, table 4-3 shows the thickness and weights of titanium (density = 0.163 lb./in^3) that would give the same level of protection as those thicknesses of aluminum in table 4-2 against a 1.8 lb fan blade fragment of the MULTI1 debris category. Note that to estimate the net weight increase of each thickness of titanium, you must subtract the weight of the corresponding thickness by the weight of the 0.04″ of aluminum and then multiply by 2. For example, the net weight increase for the 0.064″ thickness of titanium is 2*(52-20) = 64 lbs.

TABLE 4-2. VOLUMES AND WEIGHTS FOR EACH ENGINE OF REQUIRED SHIELDING FOR DIFFERENT ENGINE NACELLE THICKNESSES

Thickness of Al	0.04 in.	0.12 in.	0.14 in.	0.48 in.	1.1 in.
Volume (in^3)	200	600	700	2400	5500
Weight (lb.)	20	59	69	235	538

TABLE 4-3. EQUIVALENT VOLUMES AND WEIGHTS OF TITANIUM FOR EACH ENGINE

Thickness Al	0.04 in.	0.12 in.	0.14 in.	0.48 in.	1.1 in.
Weight Al (lb.)	20	59	69	235	538
Thickness Ti	0.02 in.	0.055 in.	0.064 in.	0.22 in.	0.51 in.
Weight Ti (lb.)	15	45	52	180	412

Figure 4-26 shows how the system contributions change based on engine nacelle thickness. The analysis results indicate that the contribution to P_{HAZ} from cross-engine debris damage (ENGINES) is slightly minimized by a nacelle thickness of 0.12″ but is almost eliminated at 0.48″. Somewhere between a nacelle thickness of 0.12″ to 0.48″ the ENGINES contribution is significantly impacted. This equates to a weight of aluminum of somewhere between 78 and 430 lbs (50 and 320 lbs of titanium, respectively).

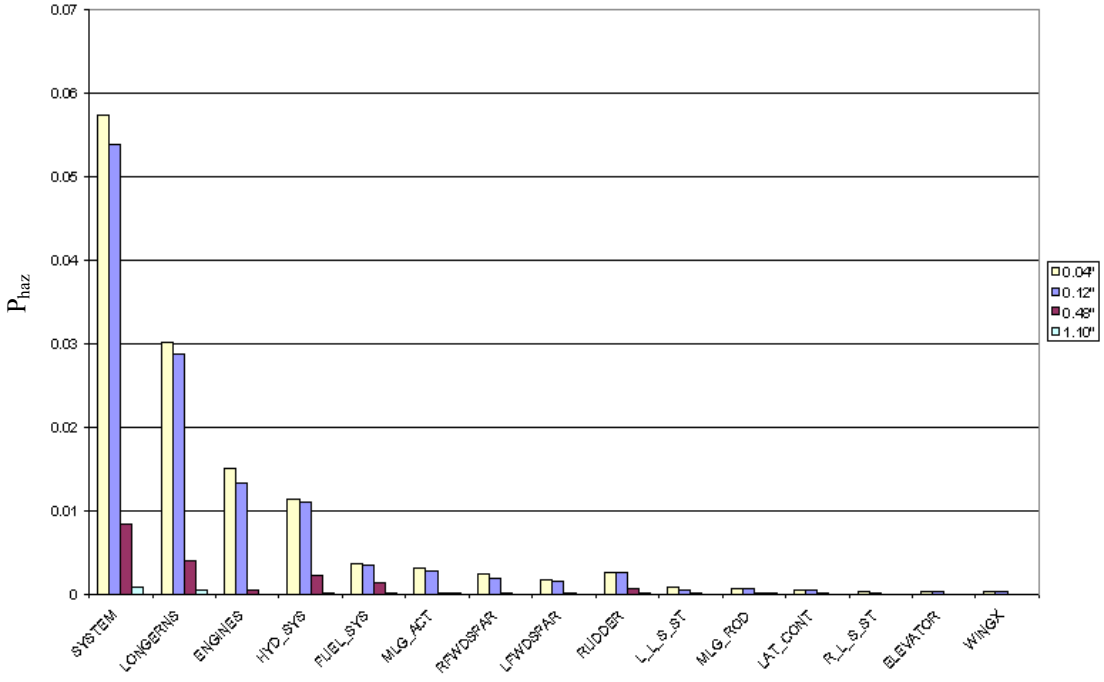

FIGURE 4-26. SYSTEM CONTRIBUTION VS ENGINE NACELLE THICKNESS

4.1.4 Generic Twin Conclusions.

The UEDDAM analysis of the GT shows that the aircraft has an overall average P_{HAZ} due to the single disk segment debris category (DISK1) of 0.043 for the baseline configuration and 0.044 for the alternate (engines lowered) configuration. This is below the AC 20-128A acceptable value of 0.050 (1-in-20) for the single 1/3 disk fragment and for the average alternate model. Note that the DISK1 debris model (see table 3-2) varies the fore/aft spread angle based on the engine section of the release, which is more representative of actual debris distributions than the AC 20-128A models. Also note that the DISK1 debris model covers a larger fore/aft spread than either the single 1/3 segment or the alternate models of AC 20-128A. While the UEDDAM DISK1 model differs slightly from the AC 20-128A models, it is more representative of a real 1/3 disk segment event and addresses the intent of the AC 20-128A models. Therefore, based on the assumptions of this analysis, the GT meets the FAA requirements for the uncontained engine debris risk for the single 1/3 disk fragment and the alternate debris model.

The UEDDAM analysis of the intermediate fragment (MFRAG) shows an overall P_{HAZ} of 0.013 and 0.016 for the baseline and alternate aircraft configurations, respectively. This is well below

the AC 20-128A acceptable value of 0.025 (1-in-40) for the intermediate fragment. Note that the MFRAG debris model (see table 3-2) also varies the fore/aft spread angle based on the engine section of the release, which is more representative of actual debris distributions and covers a larger fore/aft spread than the intermediate fragment model of AC 20-128A. In addition, the MFRAG masses exceed 1/30 of the corresponding bladed disk masses, which is the AC 20-128A required size for intermediate fragments. While the UEDDAM MFRAG model differs slightly from the AC 20-128A model, it is more representative of a real intermediate fragment event and addresses the intent of the AC 20-128A model. Therefore, based on the assumptions of this analysis, the GT meets the FAA uncontained engine debris risk requirements for the intermediate fragment.

This study did not investigate the multiple disk fragment model discussed in AC 20-128A; therefore, conclusions as to the ability of the GT to meet the AC 20-128A requirements cannot be drawn without further analysis.

The alternate aircraft configuration (engines lowered) increased the catastrophic risk probabilities for all four debris categories assessed and is, therefore, a less preferred option, although this increase did not exceed any AC 20-128A requirements.

Although the design meets the AC 20-128A requirements, there are some trends in the data that identify areas for improvement to reduce the risk of uncontained engine events. For the DISK1, MULTI, and the MFRAG debris categories, the three leading contributors to catastrophic damage are, the fuselage longerons, engines, and hydraulic system. By toughening the fuselage structure, a great reduction in risk can be achieved. While the engines are the second leading contributor, other than moving the engines farther apart or adding shielding, not much else can be done to reduce their contributions. Rerouting the hydraulic system and adding additional redundancies can achieve a moderate reduction in risk. The SINGL debris category risk values are extremely low and can be further reduced through shielding. In fact, shielding can potentially lower the risk values for all debris categories, but imposes a cost in terms of weight.

The nacelle skin thickness sensitivity study showed a significant reduction in risk to uncontained engine debris could be achieved through shielding alone. For example, by increasing the engine nacelle thickness from 0.04 to 0.14 inch, even the MULTI1 debris type catastrophic risk value is expected to decrease to the 1-in-20 value. A rough estimate shows that the increase in weight for this reduction would be approximately 100 lbs using aluminum to provide the shielding. By optimizing the nacelle thickness based on engine section, and using advanced armor materials, the weight penalty could be reduced.

4.2 GENERIC BUSINESS JET.

4.2.1 Convergence.

Two approaches were taken in examining the convergence for the GBJ runs. The first examined only the 1-in-20 analysis values. However, as stated previously, the individual results for each case are also significant. Therefore, the fan P_{haz} convergence was also examined.

A random seed is specified by the user in the control file. This seed is used by UEDDAM to generate the shotline trajectories and to allow for repeatability by using the same random numbers to generate the shotlines for various runs. The number of shotlines required to conduct an analysis will vary, depending on the size of the hazard zone and the target size. The variance of the P_{haz} for a given number of iterations selected was examined based on three production runs, all of which utilized the same configuration and input files, but different random seeds. The random seeds (A) 2501, (B) 7406, and (C) 0003 were used for this comparison. The random seed 2501 was used for all other cases in this analysis and trade study.

The three runs with all parameters except for the random seeds were compared before and after the 1-in-20 averaging was performed. The majority of the cases were within 20%-30% of an equivalent case. A few cases resulted in percent differences as high as 130%-200%. However, the 1-in-20 average (absolute value) percent difference for the aircraft P_{HAZ} was 2.2%, with the largest percent difference in the aircraft P_{HAZ} values for the three cases run being 5.6% (see table 4-4). The percent difference equation used for these comparisons was the difference between the two values divided by the average of the two values. Therefore, the large percent difference in the small fragment cases may be caused by small changes to the P_{HAZ} being more amplified by the percent difference equation than those debris categories with higher P_{HAZ}.

TABLE 4-4. PERCENT DIFFERENCE FOR IN AIRCRAFT P_H FOR RUNS WITH THREE DIFFERENT RANDOM SEEDS (A, B, AND C)

	Seeds A-B	Seeds B-C	Seeds A-C
DISK1	-4.58%	-0.70%	-3.88%
MULTI	-1.14%	-2.20%	1.06%
MFRAG	3.97%	5.57%	-1.60%
SINGL	1.30%	-2.20%	3.50%

Due to the large differences in the rotor level P_{haz} for runs where different random seeds were used, a closer examination was done for a single case. The fan was examined at the V1 to V1+30 phase of flight over 360º (72 release angles), specifying only five iterations per release angle for each DISK1, MULTI, and MFRAG debris category. The results for the 25 iterations (per release angle) runs for the three random seeds used above were also incorporated into the convergence data. The results for the smaller test case to examine convergence matched those of the production run comparison. Twenty-five iterations resulted in a variance of approximately ±20%. The results of the fan-only comparisons indicate that 50 iterations or more result in a variation of less than ±2% for the 1/3 fan disk section and intermediate fragment cases (see figure 4-27).

Because the UEDDAM small fragment debris type was used for the SINGL debris category, the results were examined separately. The runs were performed using the same configuration as the other debris categories, but 20 iterations were specified since the small fragment debris type only uses a single shotline to represent the fragment. The results show that for 120 or more iterations, the variation is less than ±2% (figure 4-28).

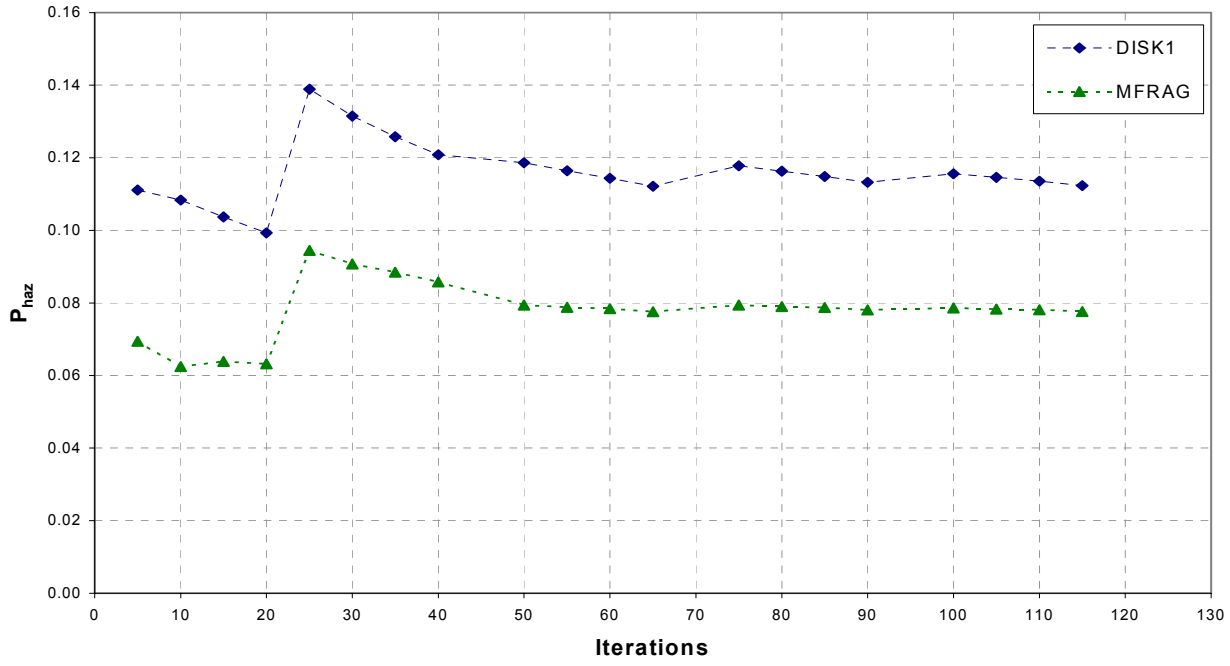

FIGURE 4-27. CONVERGENCE FOR ROTOR P_{haz} (LEFT ENGINE FAN, V1 TO V1+30, 72 RELEASE ANGLES)

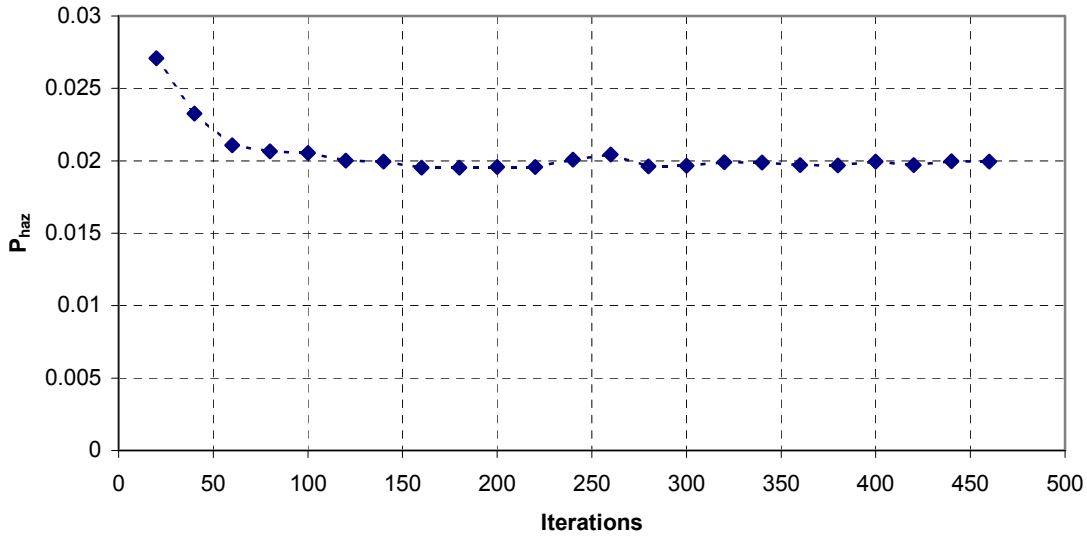

FIGURE 4-28. CONVERGENCE FOR ROTOR P_{haz} (LEFT ENGINE FAN, V1 TO V1+30, SINGL DEBRIS CASE, 72 RELEASE ANGLES)

The test for convergence should be run for each rotor of new target model because the size of the hazard zones will change, thus changing the number of iterations required to fully represent the possible shotlines.

Though the 1-in-20 values were within ±6% percent difference, the analysis of the fan P_{haz} convergence indicated that the number of iterations used in the analyses were insufficient. Despite these results, only 25 iterations (and 100 for the single small fragment) were used to reduce the run time. This results in 194,400 iterations for a full run on a single configuration. The number of shotlines for these cases will depend on the number of nodes on the shotline grid specified by the debris characterization record for segment and large fragment debris types. Because the purpose of these analyses was aimed more towards exercising the code and examining the capabilities, representative, but not necessarily certification level, values were needed. Also, the same random seed was used for each of the cases for all of the production runs, so the shotlines for each case were identical.

4.2.2 Baselines.

The relative contribution of each component to the overall P_{HAZ} of the system was consistent for all of the baseline runs (figures 4-29 through 4-31). Damage to the opposite (nonevent) engine was the largest contributor to the aircraft P_{HAZ} for both 1/3 disk section and single small fragment debris categories. The engines and the structure were the next most vulnerable to catastrophic damage from 1/3 disk sections from the first five rotors (Fan, LPC2, HPC1, HPC2, and HPC3). Debris from the four aft rotors (HPT and LPT sections) primarily affect the P_{haz} contribution of the opposite engine, aft engine beam, and structure. Catastrophic damage from severed fuel supply and fuel motive lines (resulting in fire) was also a major contributor to the fan P_{haz} (rotor) for the 1/3 disk section debris category.

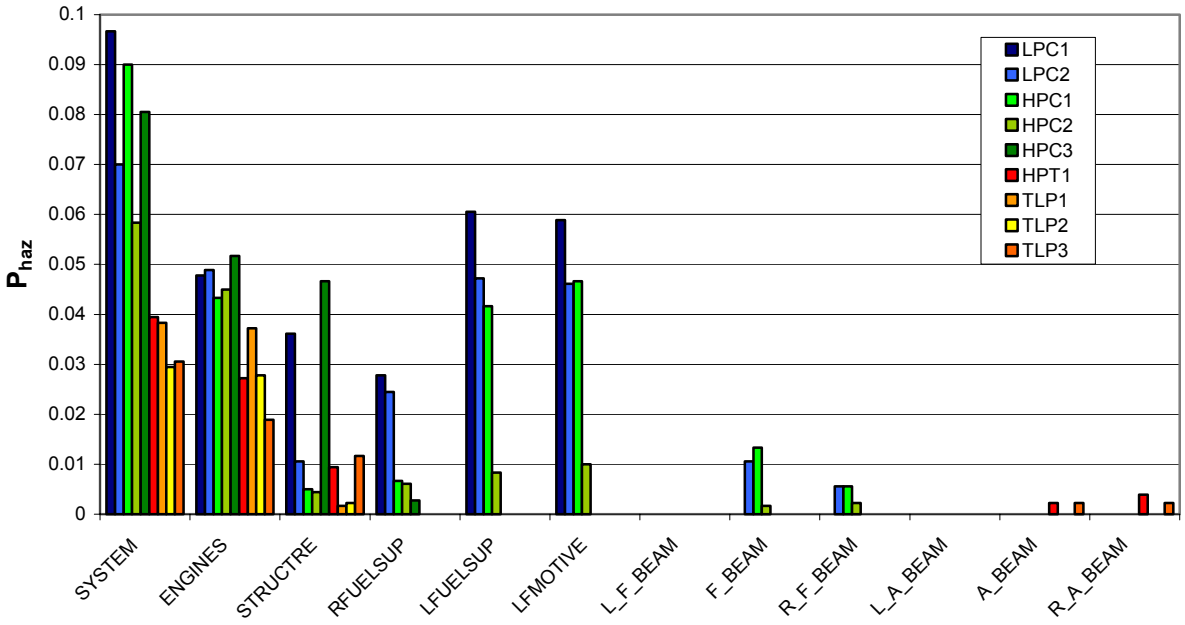

FIGURE 4-29. ONE-THIRD DISK SECTION COMPONENT CONTRIBUTION TO P_{haz} (LEFT ENGINE BASELINE, V1 TO V1+30 SECONDS)

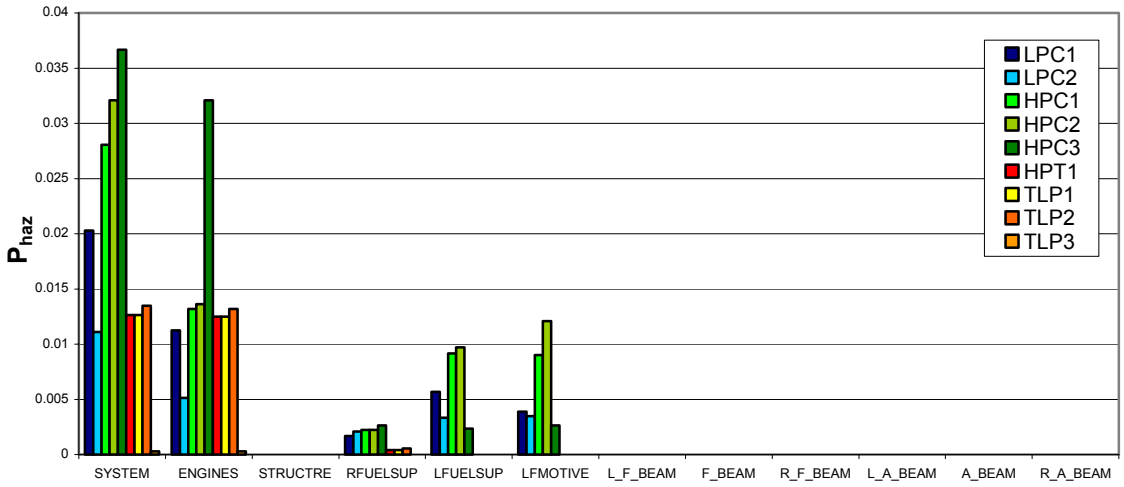

FIGURE 4-30. SINGLE SMALL FRAGMENT COMPONENT CONTRIBUTION TO P_{haz} (LEFT ENGINE BASELINE, V1 TO V1+30 SECONDS)

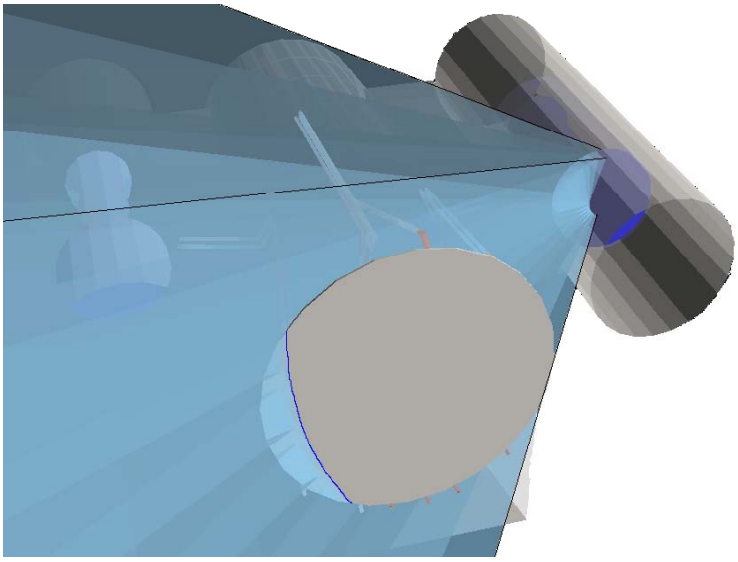

FIGURE 4-31. HAZARD ZONE FOR FAN (SINGLE SMALL FRAGMENT DEBRIS CATEGORY)

The turbine section is aft of the fuel supply and motive lines, thus the small fragments from the turbine section do not endanger the fuel lines as much as the forward (fan/compressor) rotors. The major contributor to P_{HAZ} for the single small fragment cases was damage to the opposite engine.

The fan (LPC1) and HPC3 were two of the largest and heaviest of the engine rotors. The size and positioning of these two rotors make them the large contributors to the overall P_{HAZ}. Although the HPT1 is heavier than the HPC3, it is located aft of the fuel lines and does not contribute as much to the engine P_{haz}.

4.2.2.1 DFM vs FAA AC 20-128 Spread Angle Specifications.

A comparison was conducted between the spread angles for uncontained engine debris specified by the AC 20-128 and the DFM. Because it was used as a baseline for the analysis, the DMF was also used as the baseline for this comparison.

In some instances the hazard zone became smaller when the AC 20-128A values were used (table 4-5). For example, the small fragment spread angles for the HTP1 changed from 20° forward and -50°aft to ±15° from the plane of rotation (specified by the DFM and FAA AC 20-128A, respectively). The major contributors to the single small fragment P_{HAZ} were the fuel lines and the opposite engine. Reducing the spread angles by 40º drastically changed the ratio of critical components to hazard zone area by focusing the hazard zone on the two most vulnerable components in the aft fuselage, the opposite engine and the fuel lines. The AC 20-128A suggested spread angles for turbine that resulted in a P_{HAZ} of almost double that of the DFM for the both the left and right engines.

TABLE 4-5. DEBRIS SPREAD ANGLES COMPARISON

COMP	SINGL				MFRAG				DISK1			
	Generic Uncontained Engine Debris Fragment Model		AC20-128		Generic Uncontained Engine Debris Fragment Model		AC20-128		Generic Uncontained Engine Debris Fragment Model		AC20-128	
	Fwd Spread	Aft Spread	Fwd Spread	Aft Spread	Fwd Spread	Aft Spread	Fwd Spread	Aft Spread	Fwd Spread	Aft Spread	Fwd Spread	Aft Spread
LPC1	21	-35	15	-15	2	-3	5	-5	2	-3	3	-3
LPC2	15	-3	15	-15	10	0	5	-5	5	-5	3	-3
HPC1	15	-3	15	-15	10	0	5	-5	5	-5	3	-3
HPC2	15	-3	15	-15	10	0	5	-5	5	-5	3	-3
HPC3	15	-3	15	-15	10	0	5	-5	5	-5	3	-3
HPT1	20	-50	15	-15	0	-12	5	-5	3	-11	3	-3
LPT1	20	-45	15	-15	5	-30	5	-5	3	-5	3	-3
LPT2	20	-45	15	-15	5	-30	5	-5	3	-5	3	-3
LPT3	0	-75	15	-15	5	-30	5	-5	3	-5	3	-3

The AC 20-128A debris characterization resulted in a larger hazard zone and higher P_{HAZ} from damage to the opposite engines and adjacent fuel lines for the LPC section. The fan disk spread angles increased from 2° forward and -3° aft to ±3° and resulted in an increase of approximately 15% in the left engine fan P_{haz} and 5% for the right engine fan P_{haz}. Most of the intermediate fragment hazard zones shifted aft or increased in size. This shift or increase in hazard zone reduced ratio of presented area of critical components to noncritical area resulting in lower P_{HAZ}.

The shotline density and probabilistic nature of the analysis might also have contributed to the differences in both the individual run P_{haz} and aircraft P_{HAZ} variations. Because the spread angle changed, the trajectories generated by UEDDAM are different despite the same random seed having been used. The overall changes for the aircraft P_{HAZ} ranged from a 3.1% increase for the 1/3 disk sections to a 25% decrease for the intermediate sized fragments.

4.2.2.2 Changes to the Debris Characterization.

A second change in the debris file was made to the MULTI debris category. The original debris file using the DFM specified a single small fragment (25% of the blade) associated with the disk burst. Based on the events used to produce the DFM, the events were re-examined to produce a

modified debris model. The small fragment size was changed to two sizes of fragments and fore/aft spread angles (table 4-6). The number of fragments remained the same, but the sizes better represented the historical data.

TABLE 4-6. CHANGES TO MULTI DEBRIS CHARACTERIZATION

Debris Category	Comp	DFM				Modified DFM			
		No. of Fragments	Weight (lb)	Forward Spread Angle	Aft Spread Angle	No. of Fragments	Weight (lb)	Forward Spread Angle	Aft Spread Angle
MULTI	LPC1	1	9.850	2	-3	1	9.850	2	-3
		27.7	0.123	15	-30	17.7	0.079	15	-30
						10	0.246	15	-30
	LPC2	1	3.130	5	-5	1	3.130	5	-5
		5	0.044	5	-25	3	0.040	5	-25
						2	0.048	5	-5
	HPC1	1	1.970	5	-5	1	1.970	5	-5
		5	0.025	5	-25	3	0.023	5	-25
						2	0.028	5	-5
	HPC2	1	1.060	5	-5	1	1.060	5	-5
		5	0.017	5	-25	3	0.015	5	-25
						2	0.019	5	-5
	HPC3	1	8.420	5	-5	1	8.420	5	-5
		5	0.204	5	-25	3	0.367	5	-25
						2	0.448	5	-5
	HPT1	1	10.470	3	-11	1	10.470	3	-11
		12	0.074	15	-60	7	0.033	15	-60
						5	0.127	15	-60
	LPT1	1	2.680	3	-5	1	2.680	3	-5
		5	0.051	5	-40	3	0.020	5	-40
						2	0.036	5	-40
	LPT2	1	3.220	3	-5	1	3.220	3	-5
		5	0.071	5	-40	3	0.028	5	-40
						2	0.050	5	-40
	LPT3	1	6.710	3	-5	1	6.710	3	-5
		5	0.091	5	-40	3	0.036	5	-40
						2	0.063	5	-40

The larger sized small fragments associated with the compressor disk burst in the modified debris file had a smaller spread angle than those in the original debris file. The new hazard zone focused more of the fragments into the area where many critical components are located, resulting in a higher P_{HAZ}. The fan fragments changed in size, but not spread angles, and resulted in lower component P_{haz}.

The two sizes of low-pressure turbine small fragments also resulted in lower component P_{haz}. The overall result was a 0.0021 (or 3.6%) increase in the overall aircraft P_{HAZ} for the new MULTI debris category compared to the run where only one size small fragment was used.

Because only the MULTI debris category was modified, all other debris category results were unchanged.

4.2.2.3 Pressure Bulkhead Criticality.

An investigation was conducted to examine the consequences of making the aft pressure bulkhead critical during cruise. This run emphasized the importance of the debris characterization. The aft pressure bulkhead was critical only during the cruise portion of the flight.

The Final Climb phase includes final climb, cruise, and initial descent. The debris file used the spread angles from the DFM report. The DFM spread angles for the fan are 21° forward and -35° aft of the plane of rotation. The FAA AC 20-128 only specifies a ±15° fore/aft spread angle criteria for uncontained blade (small fragment) events.

The intercept file indicates that the pressure bulkhead would be in the hazard zone for release angles of 355° to 50° (±5°) for the left engine and 140° to 210° (±5°). The pressure bulkhead was outside the hazard zone for the remaining rotors.

Because the single small fragment debris case for the fan were the only category and engine rotor to effect the pressure bulkhead, the change in P_{HAZ} was very small (1.83e-5) and resulted in a change to the baseline P_{HAZ} due to a single small fragment of less than 0.3%.

4.2.3 Skin Thickness Increase.

The skin thickness of the aft section of the GBJ was increased to protect the structure and opposite engine from uncontained engine debris. For this trade study, the skin thickness was varied from 0.032″ (baseline) to 0.080″ thick aluminum in increments of 0.016″. The three configurations of 0.048″, 0.064″, and 0.080″ thick skin resulted in an increase of 44 lb, 88 lb, and 133 lb, respectively.

Table 4-7 presents a summary of the UEDDAM results for increasing skin thickness. Increasing the skin thickness from 0.032″ to 0.08″ thick aluminum reduces the P_{HAZ} by 37% for the single small fragment debris category. The increased thickness provides a small reduction to the P_{HAZ} for the 1/3 disk case and intermediate fragment debris categories. The percent differences calculated to illustrate the reduction are important figures, but can be deceiving. It is important to realize that though the increased skin thickness reduced the P_{HAZ} for the small fragment by 37%, the actual reduction in P_{HAZ} (0.00352) is relatively small because the baseline P_{HAZ} was small. The reduction in P_{HAZ} for the 1/3 disk section was almost 0.001 but only reduces the P_{HAZ} by 2.09% of the baseline hazard level.

TABLE 4-7. SKIN THICKNESS STUDY AIRCRAFT P_{HAZ} RESULTS*

Skin Thickness	Baseline (0.032″)	0.048″		0.064″		0.08″		Hybrid	
		P_{HAZ}	ΔP_{HAZ}%	P_{HAZ}	ΔP_{HAZ}%	P_{HAZ}	ΔP_{HAZ}%	P_{HAZ}	ΔP_{HAZ}%
1/3 Disk	0.04588	0.04587	-0.03%	0.04581	-0.17%	0.04492	-2.09%	0.04547	-0.91%
Multiple	0.06853	0.06612	-3.52%	0.06452	-5.85%	0.06148	-10.29%	0.06485	-5.38%
Intermediate Fragment	0.03745	0.03723	-0.58%	0.037	-1.20%	0.03568	-4.74%	0.03623	-3.25%
Single Fragment	0.00962	0.00838	-12.84%	0.00735	-23.62%	0.00606	-37.03%	0.00614	-36.19%

*ΔP_{HAZ} indicates change from baseline values

The small changes in P_{HAZ} to the 1/3 disk section and intermediate fragment debris categories are mostly due to reductions in the contribution to P_{HAZ} from the fan (figures 4-32 and 4-33). This slight decrease in P_{HAZ} for the first stage fan was largely due to reductions in the contribution to P_{HAZ} from structural damage. Because the engine debris must penetrate five out of eight consecutive stringers, the increases in skin thickness combined with the larger area of the blade and multiple penetrations, reduces the energy of the disk sections. The increased skin thickness effectively stops many of the small fragments from penetrating the fuselage, resulting in a reduction in the contribution to P_{HAZ} from damage to the opposite engine for the single small fragment category (figure 4-34). However, the skin thickness modifications have a very limited effect on the contribution of the fuel lines to system P_{HAZ}.

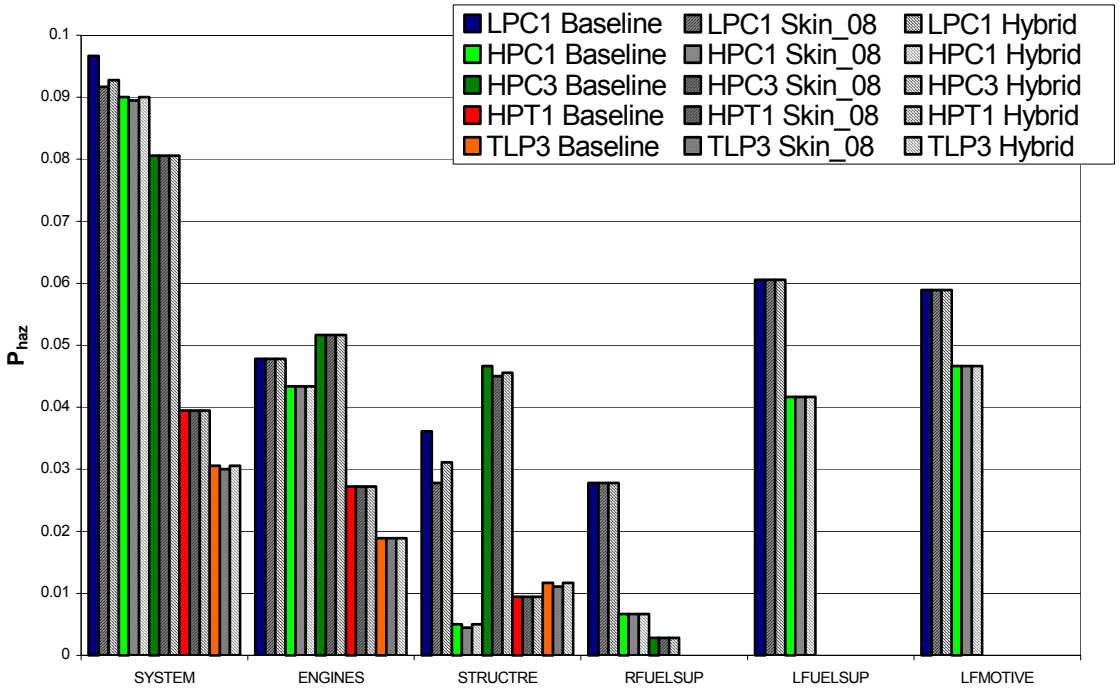

FIGURE 4-32. COMPONENT CONTRIBUTION FOR INCREASED SKIN THICKNESS (1/3 DISK CASE, V1 TO V1+30 SECONDS)

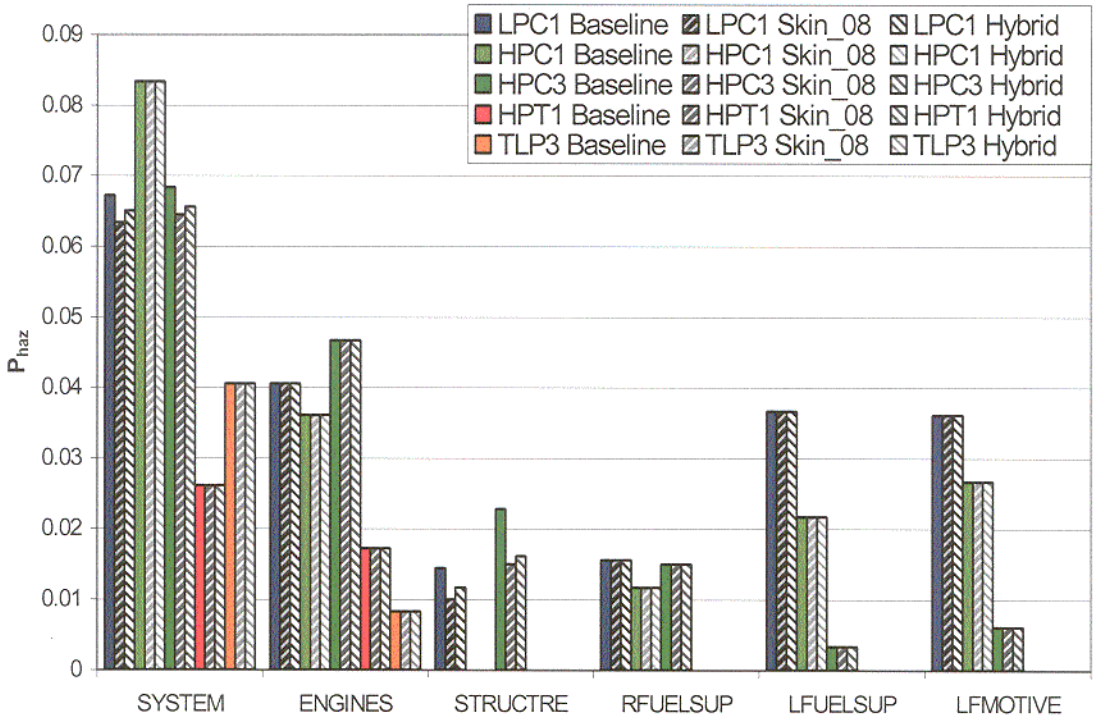

FIGURE 4-33. COMPONENT CONTRIBUTION FOR INCREASED SKIN THICKNESS (LEFT ENGINE, V1 TO V1+30 SECONDS, INTERMEDIATE FRAGMENT CASE)

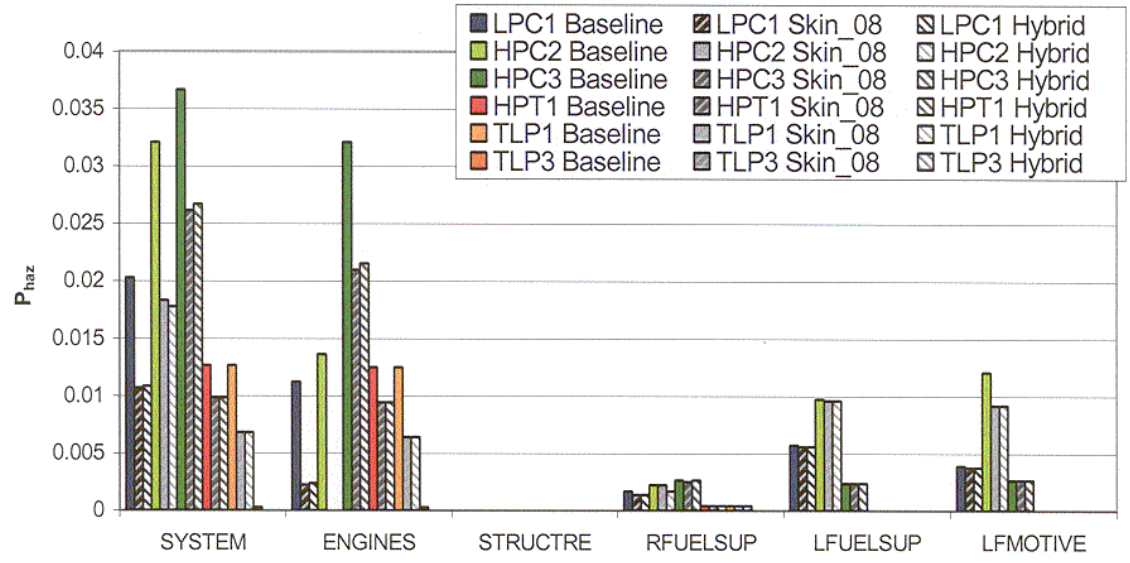

FIGURE 4-34. COMPONENT CONTRIBUTION FOR INCREASED SKIN THICKNESS (LEFT ENGINE, V1 TO V1+30 SECONDS, SINGLE SMALL FRAGMENT CASE)

The sensitivity of P_{HAZ} to weight was calculated for each of the cases. This was done by calculating the ratio of the change in P_{HAZ} to weight added to the aircraft by the additional shielding. Based on these three configurations, the sensitivity of P_{HAZ} reduction per lb of shielding weight added is highest for the 0.08″ in thick skin. However, the addition of 133 lb of shielding to the aircraft due to the increased skin thickness is a source of concern. Because any one of these modifications to the fuselage skin would add considerable weight to the aircraft (44 lb to 133 lb), these results emphasized the need to examine more localized armor for critical components.

To reduce the amount of weight added to the aircraft, an alternate configuration, called hybrid, was modeled. The modification to the skin was limited to increasing the skin adjacent to the engines to 0.080″ thick aluminum. The engines are mounted in such a way that the tops of the engines are very near the same height as the top of the fuselage. Therefore, the area directly between the two engines encompasses almost the entire top half of the fuselage (indicated in orange in figure 4-35). The length of the shielded area was 60″ with two sections extended to 70″ to shield the section of the fuel lines inside the hazard zone. Because of the location of the engines, most of the top half of the GBJ fuselage was within the cross-engine damage area. Increasing the skin thickness in these areas would provide additional protection to the opposite engine and fuel lines as well as the upper fuselage structure. The results of this modification were within 1% of the P_{HAZ} values for the 0.080″ skin for the small fragment and intermediate fragment debris categories. The change in the P_{HAZ} went from -2.09% to -0.91% for the 1/3 disk section and from -4.74% to -3.25% for the hybrid skin (a change in aircraft P_{HAZ} of 0.0013 and 0.0055, respectively). The additional weight of 16 lb is significantly lower than the 0.080″ thick skin, which weighed 133 lb, while maintaining a similar reduction in P_{HAZ} from small fragments.

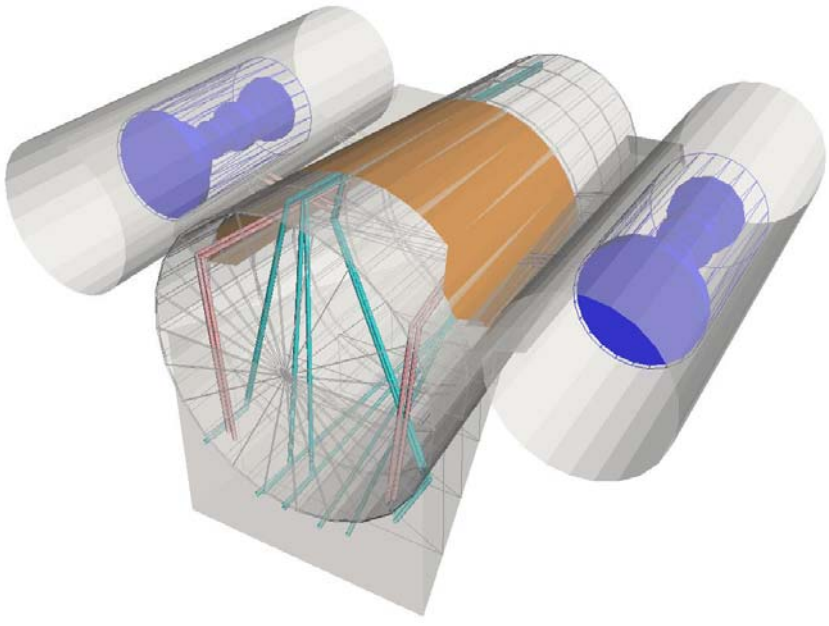

FIGURE 4-35. GENERAL BUSINESS JET MODEL WITH LOCALIZED SKIN THICKNESS INCREASE (HYBRID)

4.2.4 Fuel Line Repositioning.

Of the three major contributors to the P_{HAZ} (the engines, structure, and fuel lines), the fuel lines are the only components that can be effectively repositioned. Therefore, rerouting of the fuel lines to take advantage of natural protection afforded by the aircraft structure was examined. Because the fuel lines were modeled as long thin cylinders along a simple path, the changes were easily made. The break point locations were moved so that the placement of the fuel lines took advantage of the existing structure. The debris had to pass through the pylons, a stringer, and in some cases, the engine beam before striking the fuel lines. The left supply and motive fuel lines were moved down several inches. The right fuel and motive lines were also moved down slightly so that they lay along a stringer, but still above the pylon (figure 4-36(a) shows the original configuration; figure 4-36(b) indicates the modified fuel line routing).

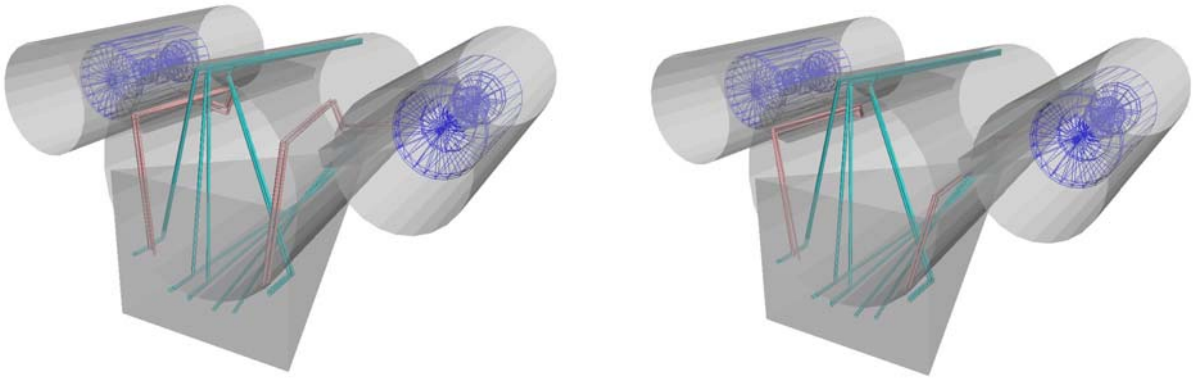

(a) (b)

FIGURE 4-36. (a) BASELINE 5 AND (b) REROUTED FUEL LINES

This configuration was only partially successful. The P_{HAZ} for the single small fragment was reduced by 30.59%. However, the P_{HAZ} for the remaining debris categories, almost all of which are several times larger than the single small fragment case, increased (see table 4-8).

TABLE 4-8. COMPARISON OF FUEL LINE REPOSITIONING RESULTS

	Baseline	Rerouted Fl	ΔP_{HAZ}	ΔP_{HAZ}%
DISK1	0.0459	0.0527	0.0051	13.31%
MFRAG	0.0375	0.0394	0.0009	2.87%
SINGL	0.0096	0.0083	-0.0021	-30.59%

Because the incremental method for P_{haz} calculation was used, multiple critical components along the same shotline do not increase the overall P_{HAZ}. Therefore, if damage to only one component along the shotline was prevented, the P_{haz} may not change because the other critical components along that shotline would still be defeated. Such was the case for this configuration. Because the engines and possibly the opposite engine fuel supply and motive lines lay on the same shotline, the repositioning of the fuel lines created a larger vulnerable area. Moving the fuel lines increased the translational risk angles by almost 10° (figure 4-37). In the original

position, the fuel lines were placed such that a shotline passing through the fuel lines would likely strike the opposite fuel supply lines or the opposite engine. The larger fragments had sufficient energy to penetrate the pylon, skin, and stringers and continued through to cause damage to the fuel lines resulting in a fire hazard. However, only one attempt was made in repositioning of the fuel lines. Because fuel lines cannot entirely be removed from the near-field area, industry standard practices suggest reducing the exposure by routing the fuel lines in the most direct route possible.

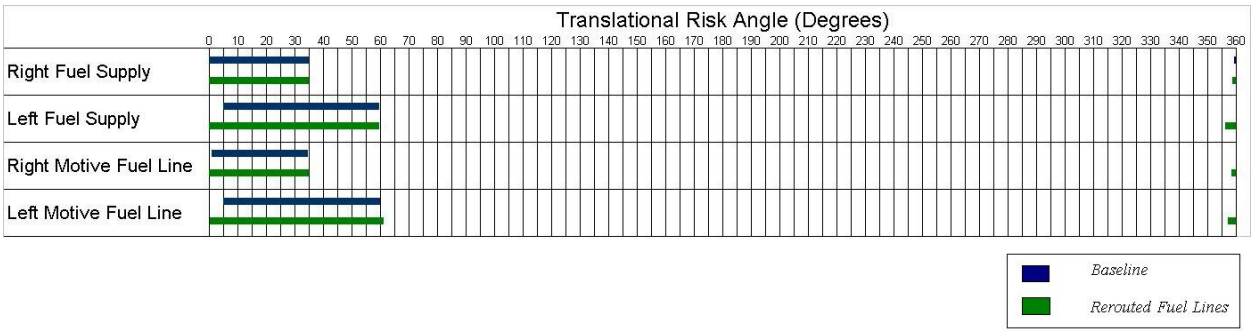

FIGURE 4-37. TRANSLATIONAL RISK ANGLES FOR FUEL LINES

4.2.5 Fuel Line Shielding.

The critical component shielding portion of this study focused on the fuel lines. The results from baseline runs revealed a high contribution to the P_{HAZ} by damage to the opposite engine, the structure, and the fuel lines adjacent to the damaged engine, resulting in fire. The localized shielding is intended to reduce the P_{HAZ} and weigh less than increasing skin thickness of the fuselage. This approach might also be easier to retrofit onto existing aircraft.

Baseline runs indicated that damage to the fuel lines from uncontained engine debris from the first four rotors were a significant contributor to the overall P_{HAZ} (up to 48%). Damage to the fuel lines adjacent to the event engine can result in a fire. Damage to the nonevent engine fuel lines would result fuel starvation and loss of thrust from the functioning engine and possibly catastrophic hazard. However, the adjacent fuel lines are larger contributors to the overall P_{HAZ}.

Two plates were used to shield the fuel lines. One plate was used to shield the horizontal section of the fuel lines; and another, smaller, plate was used for the vertical section (figure 4-38). The horizontal plates were approximately 7.5″ wide, tapering to 6.5″ at the aft end and approximately 42″ long. The vertical plate measured 9″ by 4″. The plate thickness and material was varied. Cases with only one of the two shielding sections (horizontal or vertical sections) in place were run to identify which part of the fuel line was the greater contributor to the P_{HAZ}. This was necessary because the fuel and motive lines were all modeled as a single component. The results indicated that approximately 13% of the contribution to the total P_{HAZ} comes from the shielding of the vertical section of the fuel lines and 29% from the horizontal section, the remaining 58% of the overall P_{HAZ} is due to structural or opposite engine damage.

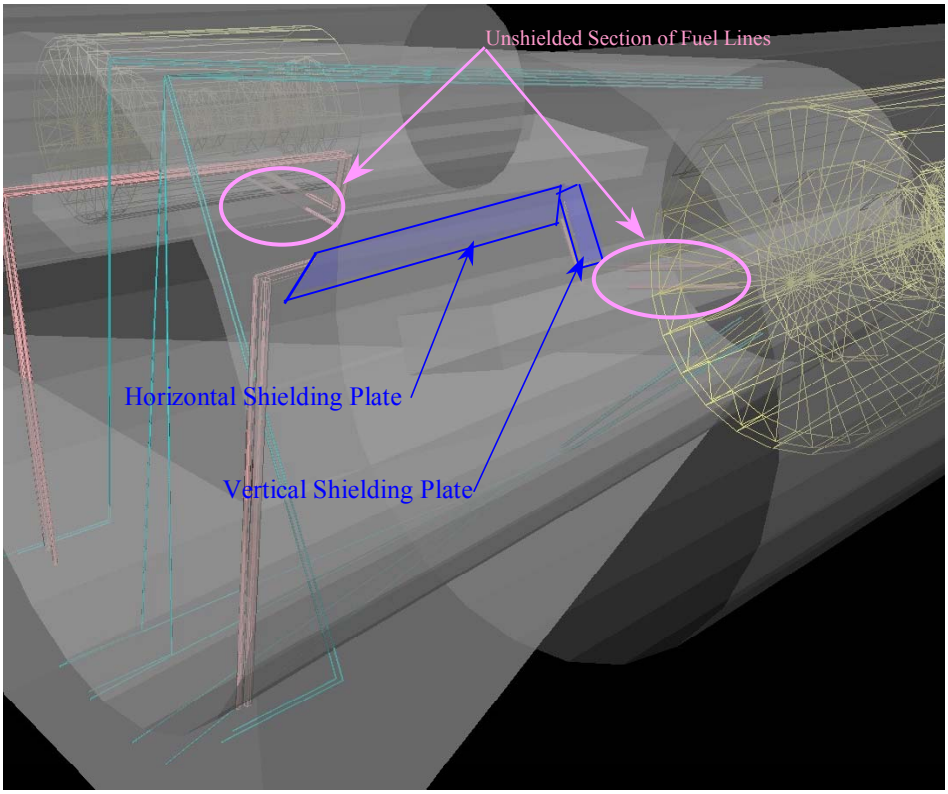

FIGURE 4-38. HORIZONTAL AND VERTICAL SHIELDING PLATES

The penetration equations were used to estimate the plate thickness required to stop the uncontained engine debris. The size, weight, and velocity of the fragments from the third stage HPC3 and steel, aluminum, and titanium plates were used for this estimation. This rotor was selected as the test case because it was one of the larger fragments and had a high P_{HAZ} relative to the other rotors for the single small fragment case. The small, intermediate, and 1/3 disk fragment characterizations were taken from the debris file.

Aluminum, titanium, and steel plates were considered for the component shielding. According to the penetration equation results, the aluminum shields had to be more than twice the thickness of either titanium or steel shielding plates to stop the HPC fragments. The titanium plates required to stop the various HPC fragments were only slightly thicker than the steel plate but much lighter (figure 4-39).

According to the penetration equation, a 0.08″ thick steel plate will result in almost the same residual velocity for a 0.11″ thick titanium plate (517 ft/s and 519 ft/s, respectively) for a given projectile size and orientation. Runs were conducted for shielding plates adjacent to the fuel lines of 0.08″ thick steel and 0.11″ thick titanium fuel. The resulting P_{HAZ} for these shielding plates were within 5% of each other. Additional runs were conducted for 0.20″ thick steel plates and a 0.24″ thick titanium plates adjacent to the fuel lines. For this case, the percent difference was less than 0.1%. From the results of this comparison, one can infer that the results from plates of one material can be applied to equivalent plates of a different material.

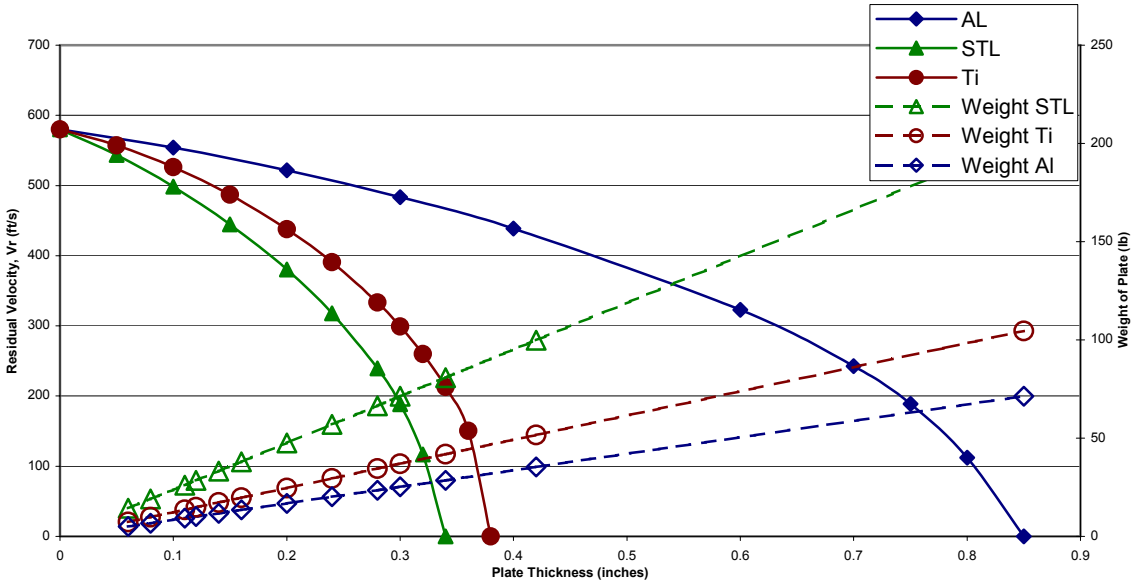

FIGURE 4-39. PLATE RESIDUAL VELOCITY AND WEIGHT COMPARISON (1/3 Disk Section)

To evaluate the potential P_{HAZ} reduction from the protecting of adjacent fuel lines from fire, a run was conducted with the fuel lines adjacent to the event engine categorized as noncritical to represent maximum shielding of the fuel lines. The probability of catastrophic hazard (fire) in the event of a hit (P_{haz}) for the fuel lines were set to 0 for the case labeled Fuel Lines NC (indicating fuel lines Not Critical with no shielding included in the target model). The addition shielding resulted in P_{HAZ} lower than that of the Fuel Lines NC configuration in some cases, and in others, the P_{HAZ} was higher than identified by the noncritical fuel line case. The shielding was meant to protect the fuel lines, but being located between two engines, it also offered limited protection to the opposite fuel lines and nonevent engine. This placement of the shielding may have resulted in the lower than expected P_{HAZ} in some cases. The cases where the P_{HAZ} was greater the noncritical fuel line case may be attributed to the small section of fuel lines between the fuselage and engine that was not shielded (figure 4-39).

The aircraft P_{HAZ} for the most effective thicknesses of titanium and steel plates are listed below in table 4-9 and plotted in figure 4-40. The highest ratio of reduction in P_{HAZ} per lb of shielding added was for the 0.18″ titanium shielding plates.

TABLE 4-9. AIRCRAFT P_{HAZ} FROM UNCONTAINED ENGINE DEBRIS FOR GBJ WITH FUEL LINE SHIELDING PLATES*

	Baseline P_{HAZ}	0.08″ Ti	0.11″ Ti	0.18″ Ti	0.22″ Ti	0.24″ Ti
1/3 Disk	0.04588	-0.17%	-0.68%	-13.67%	-19.07%	-19.07%
Intermediate Fragments	0.03745	-3.59%	-7.47%	-26.65%	-26.65%	-26.65%
Single Fragments	0.00962	-37.77%	-39.14%	-39.14%	-39.14%	-39.14%

* Percent difference from baseline values.

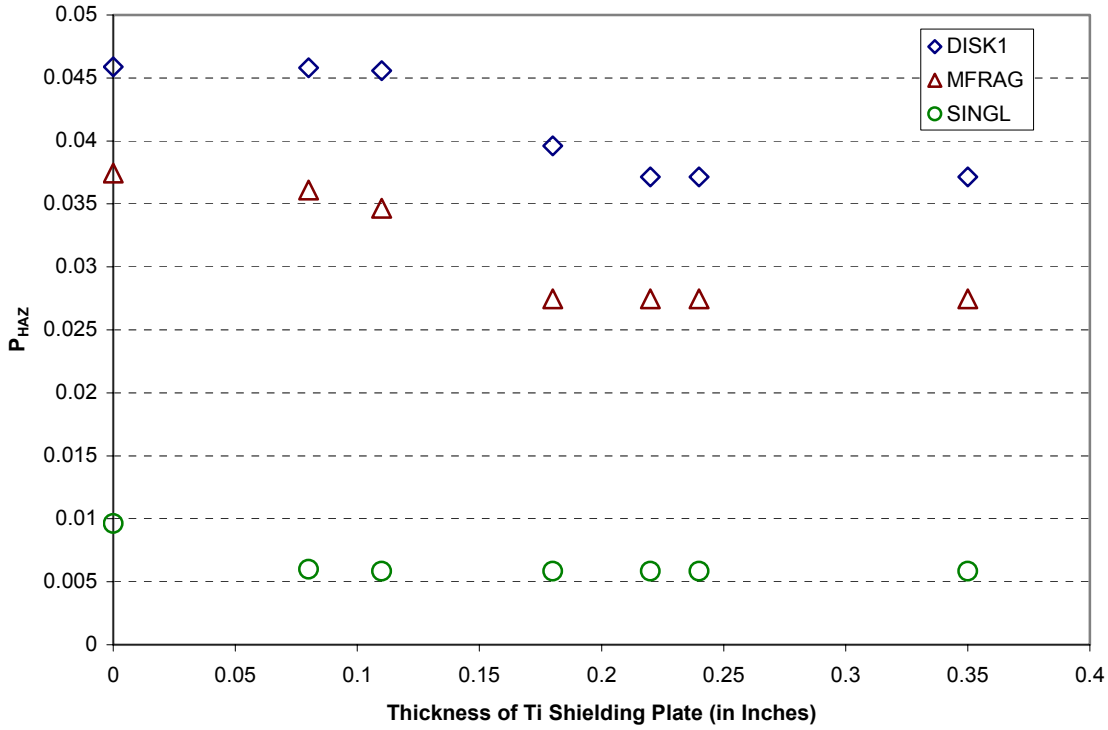

FIGURE 4-40. OVERALL P_{HAZ} FOR GBJ WITH TITANIUM FUEL LINE SHIELDING PLATES

The shielding plates reduced the P_{HAZ} for the aircraft by almost eliminating the contribution of fuel lines adjacent to the event engine. The results for a left engine disk event with the 0.22″ thick titanium shield indicate no contribution to P_{HAZ} from damage to the left fuel lines, a reduction in P_{HAZ} of approximately 0.06. However, because the incremental method for P_{haz} calculation was used, the effects of this reduction in component P_{haz} are reduced in the system (rotor) and overall P_{HAZ} (figure 4-41).

A significant contribution to the reduction of P_{HAZ} is due to decrease in the component P_{haz} resulting from damage from the fan. Though the shielding is intended to provide protection to the fuel lines, the plates also offer limited protection to opposite engine and structure (figures 4-41 through 4-43).

The shield did not stop all of the small fragments from damaging the fuel lines. This may be due to the small, unshielded portion of the fuel lines from the fuselage to the engine.

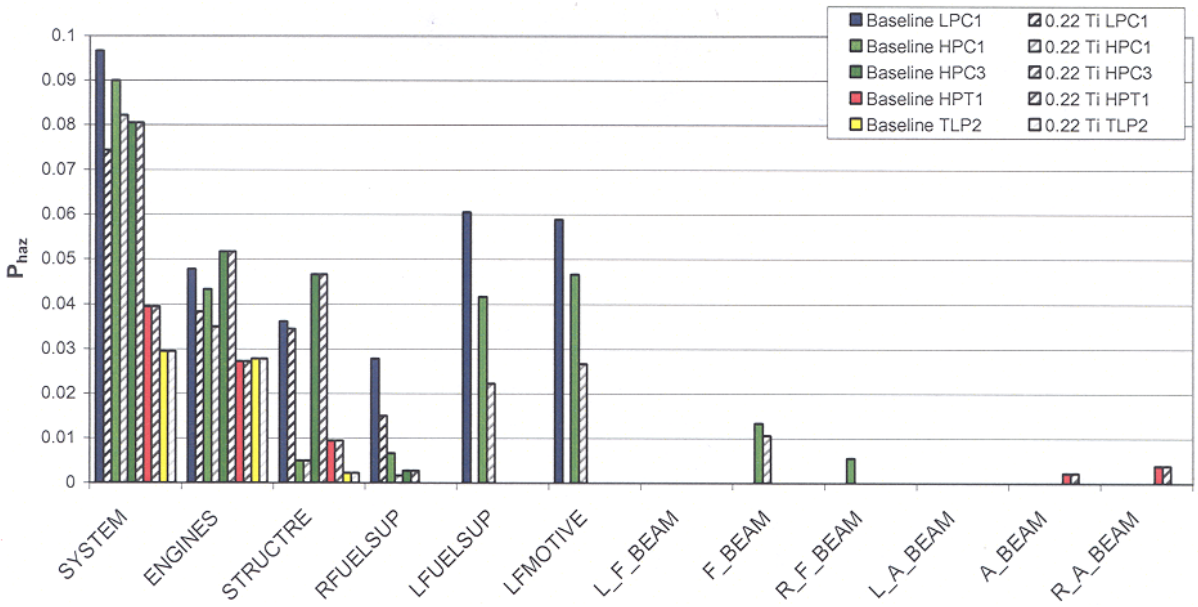

FIGURE 4-41. COMPONENT CONTRIBUTION WITH FUEL LINE SHIELDING FOR GBJ (LEFT ENGINE, V1 TO V1+30, 1/3 DISK)

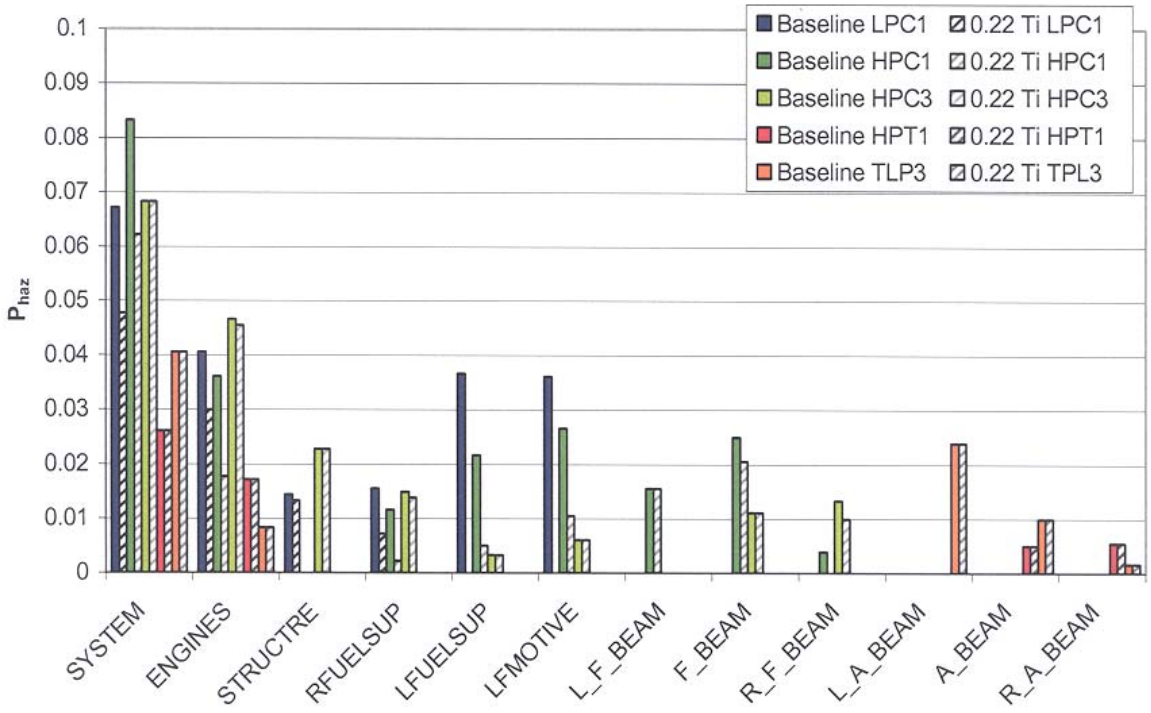

FIGURE 4-42. COMPONENT CONTRIBUTION WITH FUEL LINE SHIELDING FOR GBJ (LEFT ENGINE, V1 TO V1+30, INTERMEDIATE FRAGMENTS)

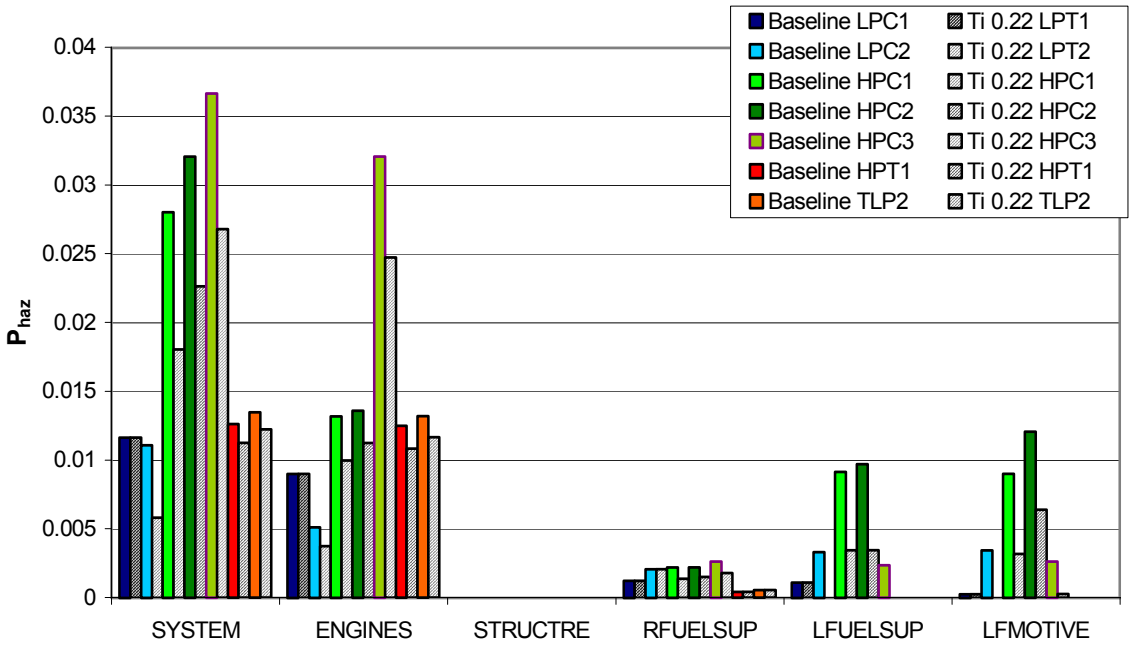

FIGURE 4-43. COMPONENT CONTRIBUTION WITH FUEL LINE SHIELDING FOR GBJ (LEFT ENGINE, V1 TO V1+30, SINGLE SMALL FRAGMENT)

4.2.6 General Business Jet Analysis Summary.

Although the increased skin thickness was effective in reducing the P_{HAZ} for all the debris cases, the increased weight may be prohibitive. Even a 50% increase in skin thickness required the addition of 44 lbs. in the aft section of the aircraft. The localized shielding resulted in a similar reduction in P_{HAZ} but weighed only 16 lb. However, increasing the skin thickness did not reduce the P_{HAZ} for the intermediate fragment to below the 1-in-40 (0.025) AC 120-28A maximum allowable P_{HAZ} for the GBJ (table 4-7).

The plates were effective in preventing the fuel lines from being severed and, hence, possible fires. Shielding of the fuel lines reduced the P_{HAZ} by up to 39% for the small fragment case, a change of 0.0038 to the P_{HAZ}. The P_{HAZ} for the intermediate fragment debris category was reduced by as much as 0.010; this represents a reduction of almost 27% of the aircraft (baseline) P_{HAZ} debris category (for shielding plates 0.18″ Ti or thicker). This shielding was slightly less effective for the 1/3 disk sections, resulting in a reduction of P_{HAZ} of 0.0088 or 19% for the 0.22″ Ti plates.

Although the component repositioning has the potential for the least weight penalty of the mitigation strategies attempted, the increase in P_{HAZ} for the larger fragments outweighed its success in stopping the small fragments.

For the sensitivity analysis, the results of each type of modification were compared based on the reduction in P_{HAZ} per pound. of weight added to the aircraft. The results indicate that the 0.22″ Ti plate resulted in the highest reduction in P_{HAZ} per pound of weight added to the aircraft for the

large and intermediate debris categories (table 4-10). The localized skin thickness increase (hybrid) resulted in the greatest reduction in P_{HAZ} due to the single small fragment debris category, but did not reduce the P_{HAZ} for the intermediate fragment to below the 1-in-40 maximum allowable P_{HAZ}. Also, the baseline P_{HAZ} for the single small fragment debris category was several times smaller than those of any other debris category examined.

TABLE 4-10. CHANGE IN P_{HAZ} PER POUND SHIELDING

	ΔP_{HAZ} per lb. Shielding			
	DISK	MFRAG	SINGL	Weight (lb.)
0.18″ Ti Plate	-2.83E-04	-4.51E-04	-1.70E-04	22
0.22″ Ti Plate	-3.23E-04	-4.70E-04	-1.39E-04	27
0.24″ Ti Plate	-2.96E-04	-4.31E-04	-1.27E-04	28
0.080″ Skin Thickness	-3.12E-06	-9.19E-06	-2.61E-05	133
Hybrid (Localized 0.080″ Skin)	-2.60E-05	-7.66E-05	-4.68E-04	16
Hybrid (Localized 0.160″ Skin)	-7.62E-05	-1.65E-04	-2.34E-04	32

The 0.22″ titanium fuel line shielding plate would constitute 27 lb of additional weight to the aircraft, including three mounting flanges on each side, and would result in as much as a 39% reduction in the P_{HAZ} from a single small fragment (table 4-11). The mounts were made of the same material and thickness as the shield and located at the fuselage frame locations.

TABLE 4-11. RESULTS FOR 0.22″ THICK TITANIUM FUEL LINE SHIELDING PLATE

	Baseline	0.24″ Ti	% Difference
DISK1	0.04588	0.03713	-19.07%
MULTI	0.06853	0.05817	-15.12%
MFRAG	0.03745	0.02473	-33.97%
SINGL	0.00962	0.00585	-39.14%

5. CONCLUSIONS AND RECOMMENTATIONS.

5.1 CONCLUSIONS.

The results of the generic aircraft analysis show that Uncontained Engine Debris Damage Assessment Model (UEDDAM) is a viable tool to assess rotor burst hazard analysis. Study results indicate that common aircraft design practices result in acceptable risk levels to realistic engine debris. Even when considering 1/3 disk segment debris trajectories out of plane of the disk rotation, values of risk probability were below the 1-in-20 requirement. This supports validation of UEDDAM in that the results show common design practices that have been proven in aircraft certification programs that meet Advisory Circular (AC) 20-128A minimization intent are also predicted by UEDDAM to be within those limits. While this is not a conclusive validation, it does shed a favorable light on UEDDAM.

One of the benefits of UEDDAM over existing manual methods is that UEDDAM automates a critical part of the AC 20-128A analysis process. Automation reduces errors, permits standardization, allows for ease of trade studies, and introduces a manageable means of evaluating uncontained engine events stochastically.

By using UEDDAM as part of the uncontained engine debris damage assessment process, a more accurate and useful analysis can be achieved. UEDDAM outputs data that allows determination of what engine sections are the major contributors to damage and, in addition, allows determination of what systems and components are responsible for the hazard. Based on this information, design improvements can be identified and prioritized. Since aircraft system and component contributions can be quantified, design improvements can be focused on specific aircraft systems. This allows for a more tailored design process that can consider more than just shielding components. For example, the analysis of the generic twin-engine aircraft (GT) showed that the hydraulic system contributed significantly to the hazard. Simply rerouting hydraulic lines and moving components can achieve a measurable reduction in risk.

UEDDAM allows for consideration of segment, intermediate, and small fragment trajectories that are out of plane of the rotor rotation. This goes beyond the common manual, infinite energy 1/3 disk segment analysis that only considers segment releases in plane with the rotor rotation. By looking out of plane, additional vulnerabilities associated with a realistic uncontained engine event can be identified and remedied. UEDDAM also considers energy reduction of all debris types. This allows for consideration of the inherent shielding effects of major structure, such as landing gear. The common manual method of assuming that the debris energy never decreases (infinite energy) does not allow for consideration of shielding effects.

UEDDAM allows for parametric studies. Once the data set has been developed, parametric studies can be performed easily by making small changes to the input and rerunning UEDDAM. This automation saves time over manual methods where parametric studies must manually repeat the entire analysis process.

Uncontained engine events are highly stochastic in nature. UEDDAM is designed to consider the stochastic nature of uncontained engine events by varying release point, debris trajectory,

and debris orientation over multiple iterations to give a more complete assessment of the threat. The fore/aft trajectory can be varied uniformly, normally, or skewed to allow better representation of real debris.

The UEDDAM visualizer aides in input development and output data analysis. The Visualizer was used in support of this analysis by plotting the components in three-dimensional space to allow analysis and discussion of the input and output data. The hazard zone plots allowed easy discovery of the limitation in shielding provided by the engine nacelle (trajectories of the turbine section debris escaped aft of the engine nacelle). While not shown in this analysis, the UEDDAM Visualizer creates plots of the translational risk angles described in AC 20-128A.

This effort has demonstrated that UEDDAM addresses the industry/Federal Aviation Administration need for an analytical tool to conduct rotor burst assessment that includes fragment penetration, system level hazard assessment, and multiple debris fragments. UEDDAM as a design tool can provide early insight to the rotor burst hazard for a given aircraft configuration. Additionally, trade studies can be performed to conduct cost/benefit analyses and minimize the rotor burst hazard. As a certification tool, UEDDAM provides a standardized approach to conduct rotor burst hazard assessment. UEDDAM output provides insight to the rotor burst hazard and can be used to develop a top level 1 in 20 analysis to address compliance to Code of Federal Regulations.

It is well understood that a rotor burst analysis is a complex analysis. UEDDAM was developed to provide useful tools to aide in conducting the analysis and presenting the results. A UEDDAM Visualizer was developed to allow visualization of the complex data and information generated from a UEDDAM run. It allows visualization of the aircraft geometry, debris hazard zones, debris trajectories, probability plots of the hazard levels, and translational risk angles.

5.2 RECOMMENDATIONS.

The lessons learned from this study show that UEDDAM has great potential to provide uncontained engine debris damage assessment in support of design and certification. This study shows promise, but it was performed by the developers who are intimately familiar with the FASTGEN and COVART. To get a better gauge of the usefulness of UEDDAM, it is recommended that an aircraft manufacturer exercise UEDDAM using the personnel that would normally do such analyses.

Use of the UEDDAM visualizer greatly enhanced data preparation and analysis but there are areas for improvement within the visualizer. The user interface is adequate but there is room for improvement. The data displayed in the visualizer was selected by the UEDDAM developers in anticipation of what the commercial aircraft manufacturers might be interested in. As part of the UEDDAM exercise described above, it is recommended that the aircraft manufacturer attempt to exercise the visualizer and document any improvement suggestions.

The rotor burst analysis is a complex process. UEDDAM provides a means to standardize this process. UEDDAM and its supporting tools are powerful, allowing for a wide variety of approaches to support uncontained engine debris damage assessment. To achieve the full power

and flexibility of UEDDAM as an analysis tool, many variables and inputs must be accurately defined and generated. It is recommended that, following the aircraft manufacturer analysis, a analysis guidelines be developed for using UEDDAM.

APPENDIX A—DEBRIS FRAGMENT MODEL TABLES

An uncontained turbine engine debris fragment model was defined using the database and fragment penetration tools developed under the FAA sponsored NAWCWPNS Uncontained Engine Debris Damage Mitigation Program. The debris fragment model is sub-divided into turboshaft, low bypass ratio (LBPR) and high bypass ratio (HBPR) engine categories. Within each category component failure types are defined and the uncontained debris characteristics provided. The model defines the average number of fragments per event, fragment size, velocity and trajectory.

The basis for this model is the *Large Engine Uncontained Debris Analysis* report and *Small Engine Uncontained Debris Analysis* report. These reports are based on historical event data to define the debris size and trajectories, specific engine characteristics and debris penetration analysis to define the fragment velocities. The event data has been analyzed and compiled into a database that can be used to define debris trends for engine categories and failure modes.

Fragment size is primarily based on damage (hole size) that has been done on aircraft. The damage dimensions were normalized to the engine component dimensions. For a fan blade event, aircraft damage was normalized by dividing the damage length by the fan blade length. Aircraft damage done by disk fragments was normalized by dividing the damage length by the disk diameter. This normalization process provides a realistic estimate of the fragment size that caused the damage, and provided a means to scale damage from one engine type to another.

The fragment model was developed to encompass a "significant majority" (approximately 85 % of the data) of the damages to the aircraft in terms of fragment size and trajectory angle. Data excluded were generally small damages at extreme trajectory angles which penetrated aircraft secondary structure only. To develop the fragment tables for each engine category and failure mode (i.e. HBPR fan blade failure) the data was sorted and plotted in a histogram based on debris size and debris trajectory (included as Appendix A). The summary of the complete data may be found in the Appendix. It should be noted that the particle sizes represent only those particles that actually struck the aircraft, and that the actual event may have produced other fragment sizes and initial velocities. The tables below represent only those particles that were documented as a threat to the aircraft.

Fragment velocity is the velocity of the fragment after it exits the cowl/nacelle structure. The analytical process defined in the *Large Engine Uncontained Debris Analysis* report was used to calculate the fragment velocity. The velocity values were based on the initial fragment-centroid velocity value with some resulting attenuation after penetrating the surrounding structure. In the cases of blade failures, a review of numerous fan blade out test results provided additional insight to the fragment velocity. High speed movie documentation confirmed that sliding frictional effects of released blade fragments against engine case structure as the fragment traveled in a forward helical trajectory would reduce their velocities to approximately 75% of the original blade tip velocity. This 75% rule was also applied to blade particles in events initiated by disk failure as well, to account for blade breakage prior to exiting the case as well as blade particle friction. This analysis was supported by one "data rich" field event where initial velocities were known and fragment size and energy were confirmed by aircraft damage

analysis. For blade initiated events, blade fragment velocities are based on penetration of the engine case, and surrounding cowl structure. For disk initiated events, blade fragment velocities are based on penetration of the engine cowl structure only (assumes the disk has compromised the engine containment case). Large disk fragment velocities (fragments weighing more than 10 lbs. are considered large) are based on initial velocity only. Small disk fragment velocities are based on the initial velocity and penetration of the engine case and cowling.

Where event data was unavailable for a failure mode for an engine type, the normalized debris size and trajectory angles from the other engine type were used. This was done in three cases:

LBPR compressor spacer-rim was scaled for HBPR compressor data
LBPR compressor disk data was scaled for HBPR compressor data
HBPR high-pressure turbine data was scaled for LBPR HPT data

Scaling of the data included accounting for different component dimensions (disk diameter and blade length), mass and rotational speeds.

Normalized Size is the fragment size divided by the blade length or disk diameter respectively.

Weight is the debris weight in pounds. The weight percentage is based on the general rotor characteristics defined in the Large Engine Uncontained Debris Analysis report Figure 3-5. Blade weight was divided by the blade weight and disk fragments are divided by disk weight. Disk rim fragments are divided by the disk weight.

Note: The engine fragment characterization tables are based upon engines installed in typical nacelle designs of the type certified in commercial transport designs of the 1970's and 1980's time period. Nacelle skin thicknesses used for the three engine types to determine residual fragment velocities are the following:

Nacelle Skin Thickness

	HBPR	LBPR	Turboprop and Turboshaft
Fan [3]	0.025 Al 0.025 Al 0.04 Al	0.04 Al	Not Applicable
Compressor	0.04 Al	0.04 Al	Disk 0.1 Steel 0.08 Steel 0.06 Al
Turbine	0.04 Al	0.04 Al	Disks 0.1 Steel 0.08 Steel 0.06 Al Blades 0.06 Al

1. Skin Thicknesses are in inches

2. Turboprop and turboshaft steel skins represent additional ducting and casing around the rotating components.

3. For HBPR fan disk events, blade fragments penetrated only the 0.04" Al.

4. For all blade containment case penetration events, the initial velocity is not reduced by 25%, and the fragments penetrate a 0.25" Steel case then the cowl.

Note: The fan blade fragment model was updated to better represent realistic debris damage characteristics. Updates were made to the number of debris for a given debris size, weight, velocity and spread angle.

Turboprop Engine Fragment Characterization

Component	Number of Events	Number of Fragments (Average/ Event)	Normalized Size	Weight (lbs)	Velocity (ft/sec) at 0° plane	Spread Angle degrees
Fan	N/A					
Compressor						
Blade Event	0	--				
Spacer - Rim	3	1				
Blades						
Rim			89%	2.6	731	±5
Disk Event	1	1				
Blades						
Disk			67%	10.2	580	±5
HP Turbine						
Blade Event	0					
Spacer- Rim	0					
Blades						
Rim	5	1	50%	0.72	541	+5 to -11
Disk Event						
Blades						
Disk	3	1	100%	8.38	533	+5 to -15
LP/PT Turbine						
Blade Event	10		63%	0.1	609	+15 to -15
Spacer- Rim	10	1				
Blades						
Rim			20%	1.05	662	+5 to -11
Disk Event	4	1				
Blades						
Disk			68%	4	572	+5 to -15

+ angles are forward, - angles are aft of the rotor plane of rotation

Low-Bypass Ratio Engine Fragment Characterization

Component	Number of Events	Number of Fragments (Average/ Event)	Normalized Size	Weight Lbs (% of total)	Velocity ft/sec at 0° plane	Spread Angle degrees
Fan						
Blade Event	2	17				
		0	10%	0.07 (2 %)		+20 to -10
		3	20%	0.3 (7 %)	907	+20 to -10
		6	30%	0.8 (19 %)	976	+20 to -10
		3	50%	2.0 (48 %)	939	+20 to -10
		5	100%	4.2 (100%)	748	+20 to -10
Disk Event	5					
Blades		17				
		6	10%	0.07 (2 %)	1102	+25 to -40
		7	20%	0.3 (7 %)	1041	+25 to -40
		1	30%	0.8 (19 %)	1021	+25 to -40
		2	50%	2.0 (48 %)	955	+25 to -40
		1	100%	4.2 (100%)	762	+10 to 0
Disks		1	100 %	41 (41%)	317	+5 to -4
Compressor						
Blade Event	2					
Spacer – Rim	2					
Blades		6.5	100%	0.25 (100%)	642	+15 to -3
Rim		2	80 %	6 (30%)	565	+15 to 0
Disk Event	6					
Blades		7.3	100%	0.25 (100%)	642	+15 to -30
Disk (Large Fragment)		1	85%	9 (45%)	334	+ 5 to -5
Disk (Intermediate Fragment)		1	30%	4 (20%)	460	+10 to -5
HP Turbine						
Blade Event	0	10	80%	0.25 (100%)	336	+20 to -50
Spacer- Rim	0					
Blades		11	85%	0.25 (100%)	871	+15 to -40
Rim		1	50%	8.5 (7%)	1000	0 to -12
Disk Event	0					
Blades		12	70%	0.25 (100%)	871	+15 to -60
Disk		1	30%	10 (8%)	743	+3 to -11

Low-Bypass Ratio Engine Fragment Characterization (Continued)

Component	Number of Events	Number of Fragments (Average/ Event)	Normalized Size	Weight Lbs (% of total)	Velocity ft/sec at 0° plane	Spread Angle degrees
LP Turbine						
Blade Event	5	8.6	50%	0.25 (37%)	378	+15 to -35
Spacer- Rim	1					
Blades		10	50%	0.25 (37%)	889	+20 to -15
Rim		1	56%	6.3 (5%)	918	+5 to -5
Disk Event	5					
Blades		23.4	50%	0.25 (37%)	889	+10 to -70
Disk		2	100%	70 (58%)	571	+3 to -5

+ angles are forward, - angles are aft of the rotor plane of rotation

High-Bypass Ratio Engine Fragment Characterization

Component	Number of Events	Number of Fragments (Average/ Event)	Normalized Size	Weight Lbs (% of total)	Velocity (ft/sec) at 0° plane	Spread Angle Degrees
Fan						
Blade Event (Helical)	11	7				
		3	10%	0.33 (3%)	904	+35 to -35
		2	20%	2.0 (16%)	895	+20 to -45
		1	30%	3.75 (30%)	877	+20 to -30
		1	50%	6.24 (50%)	808	+15 to -30
		0	70%	8.61 (70%)		
		0	100%	12.5 (100%)		
Disk Event	3					
Blades		27				
		10	10.0%	0.33 (3%)	935	+10 to -30
		9	20.0%	2.0 (16%)	928	+15 to -25
		2	30.0%	3.75 (30%)	894	+10 to -25
		4	50.0%	6.24 (50%)	822	+10 to -20
		1	70.0%	8.61 (70%)	796	+10 to -20
		1	100.0%	12.5 (100%)	644	+15 to +5
Disks		3	100%	45 (38%)	303	+2 to -3
Compressor						
Blade Event	0					
Spacer – Rim	1					
Blades		6.5	100%	0.25 (100%)	642	+15 to -3
Rim		2	80%	6.0 (30%)	523	+15 to 0
Disk Event	2					
Blades		4.5	50%	0.19 (76%)	609	+5 to -25
Disk (Large Fragment)		1	85%	9 (45%)	380	+5 to -5
Disk (Intermediate Fragment)		1	30%	4 (20%)	385	+10 to -5

High-Bypass Ratio Engine Fragment Characterization (Continued)

Component	Number of Events	Number of Fragments (Average/ Event)	Normalized Size	Weight Lbs (% of total)	Velocity (ft/sec) at 0° plane	Spread Angle Degrees
HP Turbine						
Blade Event	1	10	80%	0.25 (100%)	337	+20 to -50
Spacer- Rim	3					
Blades		11	85%	0.25 (100)%	871	+15 to -40
Rim		1	50%	10 (83%)	967	0 to -12
Spacer		1	50%	2 (16%)	781	+20 to -37
Disk Event	5					
Blades		12	70%	0.25 (100%)	871	+15 to -60
Disk		1	30%	10 (8%)	967	+3 to -11
LP Turbine						
Blade Event	8	6.5	50%	0.25 (37%)	212	+20 to -45
Blade Event Last Stage	4	6.5	50%	0.25 (37%)	200	0 to -75
Spacer- Rim	2					
Blades		5	15%	0.05 (7%)	326	+6 to -20
Rim		1	20%	11.3 (9%)	505	+5 to -5
Disk Event	1					
Blades		5	28%	0.25 (20%)	313	+5 to -40
Disk		1	20%	18 (15%)	535	+3 to -5

+ angles are forward, - angles are aft of the rotor plane of rotation

The uncontained failure event rates by component set forth in the Table below are taken from the AIA PC 342-1, Committee on Continued Airworthiness Assessment Methodology (CAAM) Supplemental Report on Turbine Engine Uncontained Events dated 5 February 1997. The event rates cover the period 01/01/1982 through 11/30/96 and are the most current rates available. The data used to characterize fragment hazards to the aircraft were obtained from all uncontained engine - aircraft events where fragment information was available, including those from earlier time periods. There is no agreement in the event counts between these two sets of data and such an agreement should not be assumed to exist. For the Table below the uncontained events for high and low pressure compressors were combined under the heading - Compressor. Similarly, the uncontained events for high and intermediate pressure turbines were combined under the heading - HP Turbine.

Uncontained Event Rate Table

	Turboprop		Low Bypass Ratio		High Bypass Ratio	
Component	Number of Events	Rate*	Number of Events	Rate*	Number of Events	Rate*
Fan						
Blade Event			26	2.2E-7	90	10.1E-7
Disk Event			8	0.68E-7	4	0.45E-7
Compressor						
Blade Event	1	0.08E-7	13	1.1E-7	2	0.22E-7
Spacer – Rim	0		6	0.51E-7	1	0.11E-7
Disk Event	10	0.84E-7	10	0.84E-7	10	1.1E-7
HP Turbine						
Blade Event	7	0.59E-7	4	0.34E-7	2	0.22E-7
Spacer- Rim	2	0.17E-7	0		4	0.45E-7
Disk Event	18	1.5E-7	0		6	0.67E-7
LP Turbine						
Blade Event	10	0.84E-7	48	4.1E-7	64	7.2E-7
Spacer- Rim	0		0			
Disk Event	5	0.42E-7	7	0.59E-7	5	0.56E-7

* Per Aircraft Flight

Based on 118.381E+6 Turboprop Aircraft Flights, 118.346E+6 Low Bypass Ratio Turbofan Aircraft Flights and 89.269E+6 High Bypass Ratio Turbofan Aircraft Flights in this calendar period.